2013

Damage Detection And Analysis In Cfrps Using Acoustic Emission Technique

Travis Laron Whitlow
North Carolina Agricultural and Technical State University

Damage Detection and Analysis in CFRPs Using Acoustic Emission Technique

Travis Laron Whitlow

North Carolina A&T State University

A dissertation submitted to the graduate faculty

in partial fulfillment of the requirements for the degree of

DOCTOR OF PHILOSOPHY

Department: Mechanical Engineering

Major: Mechanical Engineering

Major Professor: Dr. Mannur Sundaresan

Greensboro, North Carolina

2013

School of Graduate Studies
North Carolina Agricultural and Technical State University
This is to certify that the Doctoral Dissertation of

Travis Laron Whitlow

has met the dissertation requirements of
North Carolina Agricultural and Technical State University

Greensboro, North Carolina
2013

Approved by:

Dr. Mannur Sundaresan Major Professor	Dr. John Kizito Committee Member
Dr. Frederick Ferguson Committee Member	Dr. Albert. Esterline Committee Member
Dr. Claude Lamb Committee Member	Dr. Arturo Fernandez Committee Member
Dr. Samuel Owusu-Ofori Department Chair	Dr. Sanjiv Sarin Dean, The Graduate School

Biographical Sketch

Travis Laron Whitlow was born on May 3, 1986, in Roanoke, Alabama. He received his Bachelor of Science Degree in Mechanical Engineering from Alabama A&M University, Normal, AL, in 2008. He joined the Mechanical Engineering Ph. D. program at North Carolina Agricultural and Technical State University in August 2008. He is a candidate for Ph.D. in Mechanical Engineering.

Dedication

This Doctoral Dissertation is dedicated to my family for their continual support though the completion of this work.

Acknowledgements

I would like to thank my academic advisor, Dr. M. J. Sundaresan, for his guidance and support and for giving me an opportunity to do research. In addition, I would like to thank to my committee members for taking the time out to review this work.

I would like to give much appreciation as well to my colleagues Dr. Kassahun Mekonnen, Letchuman Sripragash, Gopal Kumaran, Dr. Hardik Vagh, Gene Warwick and other members of Intelligent Structures and Mechanisms (ISM) laboratory. I also would like to thank Katrina Emery, Lance Richards, Larry Hudson, Allen Parker, Patrick Chan, and other NASA personnel who made this research possible

Table of Contents

List of Figures

List of Tables

Abstract

Real time monitoring of damage is an important aspect of life management of critical structures. Acoustic emission (AE) techniques allow for measurement and assessment of damage in real time. Acoustic emission parameters such as signal amplitude and duration were monitored during the loading sequences. Criteria that can indicate the onset of critical damage to the structure were developed. Tracking the damage as it happens gives a better analysis of the failure evolution that will allow for a more accurate determination of structural life. The main challenge is distinguishing between legitimate damage signals and "false positives" which are unrelated to damage growth. Such false positives can be related to electrical noise, friction, or mechanical vibrations. This research focuses on monitoring signals of damage growth in carbon fiber reinforced polymers (CFRPs) and separating the relevant signals from the false ones. In this Dissertation, acoustic emission signals from CFRP specimens were experimentally recorded and analyzed. The objectives of this work are: (1) perform static and fatigue loading of CFRP composite specimens and measure the associated AE signals, (2) accurately determine the AE parameters (energy, frequency, duration, etc.) of signals generated during failure of such specimens, (3) use fiber optic sensors to monitor the strain distribution of the damage zone and relate the changes in strain measurements to AE data.

CHAPTER 1

Introduction

All man-made structures (i.e. bridges, automobiles, and airplanes) will experience various types of loading throughout their lifetime. The loading may exceed the strength of certain components of the structure and cause them to fail or a component may be worn out over time due to fatigue loading. In either case, damage will initiate and propagate if such loading is continued. The presence of damage reduces the strength of structures and can possibly affect it's performance. In order to keep structures up to standard from both a safety and operation standpoint, techniques are needed to constantly assess the integrity of the structure.

Several non-destructive techniques (NDT) have been developed to assess the extent of damage in structures. However, these techniques do require disassembly and can miss critical damage growth between periodic inspection. Real time monitoring techniques, usually termed structural monitoring techniques, can be implemented to continuously monitor a structure. Acoustic emission (AE) has the potential to be used as an SHM tool. Acoustic emission techniques have been around for decades and while AE is able measure damage as it happens, the inability to consistently differentiate between indicators related to real damage from extraneous signals has prevented them from being implemented. Minimizing the uncertainty of AE signals will greatly increase the possibility of acoustic emission being used to monitor critical structures. This research attempts to identify critical AE signals among a very large volume of AE data that are usually collected.

Several topics mentioned above serve as motivation for this work which focuses on three aspects of damage assessment. These are the measurement and optimal analysis of acoustic emission signals, relating AE signals to the severity of damage, and how damage growth affect

the local strain distribution within a material. The materials used in this research include two different layups of carbon fiber reinforced polymers (CFRPs): cross-ply and quasi-isotropic. The following sections of this chapter include an overview of NDT techniques, a background of this work, and the outline of this manuscript.

1.1 Non-Destructive Evaluation and Structural Health Monitoring

Detecting damage in a structure is critical to assessing it's life. Aircrafts go through periodic maintenance and are routinely inspected to ensure that the structure is able to perform within a predetermined measure of safety. Various none destructive evaluation (NDE) techniques are used to inspect aircraft components and several can be seen in Table 1.1. NDE techniques rely on basic principles to inspect and detect discontinuities in a structure. Energy is introduced or extracted in various forms and a response is measured and interpreted. If the part has been in service, the response is normally compared to a baseline that was gathered after fabrication. Comparing the response to the baseline could give an indication of how much damage, if any, has occurred. Acoustic emission monitoring involves measuring the sound waves released during damage growth in structures when they are loaded. The sound waves released can be measured with a variety of sensors. Based on the information gathered, an assessment can be made about the structural integrity. This is important in determining whether the structure is safe enough to return to service. In this role, acoustic emission based SHM techniques can complement NDE techniques and compensate for some of their limitations while reducing the cost of maintenance and downtime.

Table 1.1.

NDE techniques

NDE Technique	Description
Acoustic Emission	Utilizes sound waves resulting damage growth
Dye Penetrant Inspection	Liquid dye penetrates part and highlights defects
Magnetic Resonance Imaging	Uses magnetic resonance to image atoms in parts
Eddy Current Inspection	Electromagnetic induction to detect damage
Ultrasonic Inspection	Ultrasonic waves used to characterize flaws
Thermographic Inspection	Thermal imaging of surface and internal structure

Real time monitoring of a structure allows for continuous assessment of the structure's state. Maintenance is based on current information and any unnecessary downtime can be avoided, thus keeping the structure in service for longer periods. There are reliability issues regarding the accuracy of any system that will be depended upon for safety. As these issues are addressed, integrated structural health monitoring (SHM) is closer to becoming a reality.

The inspiration of SHM was drawn from the human nervous system. Nerves course throughout the body and act as millions of distributed sensors. In structures, there will be a limitation on the number of sensors but the methodology is the same. An embedded sensor network will consistently monitor the state of the structure and detect any damage as it happens. Structural damage assessment in composite laminates can be divided into damage location, classification, and quantification.

SHM techniques can be passive or active. Active systems such as ultrasonic guided wave techniques utilize transducers to propagate waves through a structure. The characteristics of the wave change as it encounters damage and the level of change can be directly related to the

amount of damage. Acoustic emission (AE) is a passive monitoring technique that relies on the strain energy generated during damage growth. A small burst of energy is released when a crack grows and propagates as stress waves within the structure. The signatures seen in these signals and the rate at which they are emitted are a function of the type of damage that has occurred and the rate at which the damage is growing, respectively.

1.2 Acoustic Emission Monitoring Technique

An acoustic emission can be defined as the sudden, rapid release of strain energy in the form of transient stress waves within a material. AE is general associated with damage growth but several mechanical processes can give rise to false emissions: friction, structural vibration, and electric noise.

The purpose of using acoustic emission techniques is to have the ability measure damage in real time. Acoustic emission sensors can be mounted on structures and monitor AE events originating from the neighboring area. Damage growth in metallic structures usually involve with a single dominant crack but damage growth in composite materials is very different. Composites have several failure mechanisms, such as matrix cracking, fiber breaks, and delamination, which occur in combination in highly stressed regions. Countless research has been done to connect AE events to these failure mechanisms. The typical aspects of damage growth in composites are given by the following:

- **Measure**: acquire AE signals within a structure as it fails
- **Analysis**: use AE features to distinguish between the type of damage
- **Prognosis**: relate the AE data to the integrity of the material

1.3 Background of the Study

Unidirectional composites are known to have different failure modes. Some of these modes or source mechanisms are matrix cracks, fiber breaks, and delamination. The physics behind each of these mechanisms are quite different and should give rise to unique AE signals at the source. Various AE parameters such as amplitude, frequency, duration, and risetime can possibly be used to isolate signals from each mode. However, there are several aspects of wave propagation that will affect the preservation of the identity of the source mechanism in the received signal. Dispersion, attenuation, scattering, and limited sensor response are some of the aspects that limit the ability to distinguish different source mechanisms. The impact of these aspects could affect measurement of amplitude, frequency, and duration; the very parameters used to determine the source mechanism. Previous work does not focus on the effect of dispersion, scattering, and etc. but to fully interpret the AE signal, these aspects must be addressed. The first part of this research examines a method of analyzing AE signals from static and fatigue loading while accounting for the previously mentioned aspects.

While detecting damage using AE technique is common, the effect of damage is not well understood. The ability of determining the remaining strength of structure during damage growth is the ultimate goal of SHM. From an AE literature review, it was seen that models can be develop to predict the fatigue life of composite. Composites fail in stages and the final failure occurs rapidly. Conventional AE techniques, while capable of detecting impending failure, are not likely to be useful in averting catastrophic failure. The second part of this research looks at a method to detect critical damage before catastrophic damage growth sets into the structure.

Damage growth in composites in much more distributed than what is seen in metals. A single dominant crack usually dominates during failure in metals. In comparison, the presence of

multiple failure modes in composites makes quantifying damage difficult. Further, damage to structures can cause interlaminar delaminations that are not detected by visual inspection. Such damage can spread and quickly degrade the load carrying capabilities of the affected area. The third part of this research utilizes fiber optic sensors to measure the changes in the strain distribution due to damage growth.

1.4 Specific objectives of the research

This research is motivated by the basic need to understand the failure process in CFRPs for structural health monitoring purposes. Composite materials have increased in popularity and usage of the past decades. However, the complex nature of failure of these materials has not been well understood. Several other aspects are considered as well. The need for real time monitoring requires the ability to extract useful information from data and give an instant damage assessment.

The overall objective is to utilize acoustic emission signals to monitor damage in CFRPs, including the following:

- **To isolate the different damage mechanisms in composite materials**

  CFRP specimens were tested under static and fatigue loads. AE signals from these tests were recorded and analyzed to isolate critical damage events.

- **To distinguish between critical and non-critical damage growth**

  Use results from specimen tests to detect critical damage growth in a CFRP panel. Only signals that correspond to significant damage growth will be analyzed

Complimentary damage detection using AE technique with fiber optic strain measurement

Ideally, having a system that is able to measure all aspects of structural integrity is desired. Combining different SHM monitoring technologies can provide a more robust approach to assure safety of critical structures. In this research, an attempt is made to combine information gathered from AE technique with results from fiber optic sensors.

The main results from this work include:

- Isolation of the different AE signals resulting from various damage mechanisms
- Monitoring of damage mechanisms and their relation to the failure process in composites.
- Relation of AE activity to change in strain field using fiber optic sensors
- Application of physics based clustering on acoustic emission signals

1.5 Research Rationale and Benefits

As composites become more and more integrated in critical structures, there is a need to develop techniques that can assure their safety. All structures degrade over time such as metals rusting or cracking. Failure of metals is well understood but composite materials have complex failures and can fail in several ways. Understanding failure in CFRP and monitoring and prediction of structural integrity is driving force behind this research. Determining which stage of the failure process the structure is currently in will allow for a better judgment on whether further inspection is needed, thus decreasing downtime.

Aviation and space applications are the main focus areas of this research. The improvement of the reliability and accuracy of SHM using AE techniques and the implementation of such technology will give the ability to make critical structures safer.

1.6 Structure of Dissertation

This dissertation has been broken down into six components. Chapter 1 provides an introduction and background on the research topics discussed later. An in depth literature review on damage evolution in composite materials, acoustic emission, and previous work relating AE features to the different failure modes is discussed in Chapter 2. Chapter 3 deals with the instrumentation, equipment, and materials used to successfully complete this research. Results from static and fatigue tests are presented in Chapter 4. Chapter 5 discusses results of SHM of a quasi-isotropic CFRP panel subjected to static load to failure. Acoustic emission technique and fiber optic strain measurements were used for monitoring the damage development in this panel. The results from fiber optic sensor sensors attached to the panel are also presented in this chapter. The final chapter, Chapter 6, gives a summary, conclusions, and recommendations of the research presented in this work. References and appendices are contain in the last section.

CHAPTER 2

Literature Review

2.1 Carbon Fiber Reinforced Polymers (CFRP)

Fiber reinforced polymers (FRP) have increasingly become in popular over the last few decades. Primary structural elements in the aerospace and civilian applications are being fabricated from FRPs due to their superior structural properties. Compared to traditional metals, such composite materials have high strength-weight and stiffness-weight ratios, superior fatigue , and are corrosion resistant.

The applicability of composite materials can be seen in early civilizations. Roman aqueducts utilized concrete, which is a mixture of cement (binding agent) and aggregate. Combing several components or constituents to make a stronger material is the hallmark of composite materials. Modern day composites gained notoriety in the early 1970s and have been consistently integrated into today's structures.

A fiber reinforced polymer is composed of two basic components, fiber and a matrix. Fibers can be made of glass, carbon/graphite, or aramid while the matrix material can be polyester, vinylester or epoxy. The two basic constituents are combined to form a single layer material or lamina. Continuous fiber composites can be either unidirectional or woven. Several laminae are stacked together and oriented in such a way that the material properties such as strength and elastic properties needed for a given application can be achieved. Table 2.1 shows a comparison of carbon fiber and conventional metals.

Table 2.1.

Comparison of carbon fiber and conventional metals

Material	Specific Gravity	Young's Modulus	Specific Modulus
Steel	7.9	200	25.3
Aluminum	2.7	76	28
Carbon (high strength fiber)	1.8	295	164

Fabrication of composite materials can have several forms depending on how and where the material is to be used. Vacuum bag, pressure bag, and autoclave are a few of the various methods used to cast the material into it's final shape.

The most common composite material is fiberglass which is comprised of glass fibers embedded in a resin matrix. It was widely used for automobiles and marine applications in the 1950s and later widely used for bumpers cars. The Boeing 707 (1950s) was comprised of approximately 2% fiberglass (Appropedia, 2013). The aerospace industry has benefited greatly from the development of composite materials. The superior properties of composite materials enabled significant improvements in the performance of aerospace vehicles. They can be used to reinforce components that are damaged in service as well as replace them. Boeing's 787 Dreamliner was the first commercial aircraft to have it major components made of composite materials, Figure 2.1.

The versatility of CFRP has led to their wide usage. When compared to conventional alloys, the high performance composites generally exhibit superior mechanical properties. A low specific gravity seen in the FRP translates to a greater strength to weight ratio. Another advantage of carbon fiber reinforced composite is their low coefficient of thermal expansion that makes the graphite/epoxy material ideal for moderately high temperature applications.

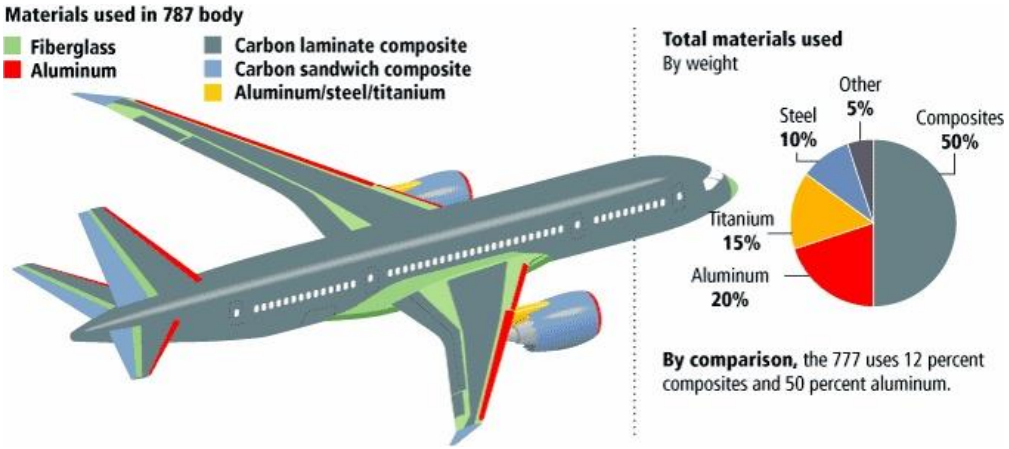

Figure 2.1. Boeing 787 Dreamliner

http://siag.project.ifi.uio.no/problems/grandine/

While composites possess stronger tensile properties than conventional metals, they have relatively weaker out-of-plane and properties and, hence, are highly susceptible to damage from impacts. Impacts may cause interlaminar delamination within the material that are not visible on the surface.

Once damage is initiated, composite materials are known to fail differently than metals. Whereas failure in metals is determined by a single dominant crack, CFRPs fail in different stages. Also, they can be affected differently by incipient defects that may play a role in the propagation of damage within the structure. In some cases, the fabrication process can introduce discontinuities within the material such as: uneven distribution of the constituents during curing, voids, or foreign particles. Storage environments with high humidity can lead to moisture absorption and decrease the strength properties of composites. The presence of such defects creates localized areas of stress concentration which can initiate fiber-matrix debonding, interlaminar delamination, or eventual premature failure.

2.2 Damage Mechanisms in Composites

As mentioned previously, there are several sources that may introduce damage into composites. Extreme loading conditions, adverse environments, age degradation, and impact from foreign objects are various ways damage can occur. Initial damage will propagate and eventually lead to the major failure modes seen in composites. Important failure modes or mechanisms are matrix cracking, fiber breakage, and delamination.

Failure modes seen in a given structure is dependent on the orientation of the plies, as well as the type of load the structure encounters. A unidirectional lamina loaded in the 0˚ direction will experience some matrix splitting but fiber breakage will be the governing failure mode, as seen in Figure 2.2.

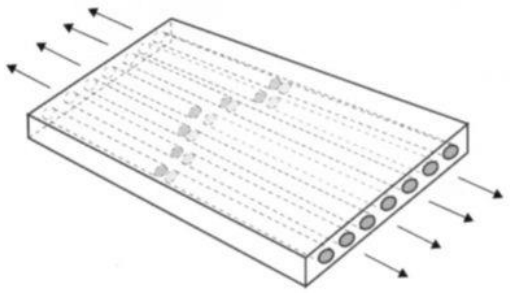

Figure 2.2. Fiber breaking (Milne, 2003)

However, if the same lamina is loaded in the 90˚ direction, transverse matrix cracking will dominate and determine the load at which failure occurs, shown in Figure 2.3. Since the matrix material is significantly weaker than the fibers, the 90˚ loaded lamina will fail at a much lower load. Damage in laminates will produce a significant amount of both matrix cracking and fiber breakage, depending on the layup. Again, these failure modes depend on the alignment with respect to the loading direction.

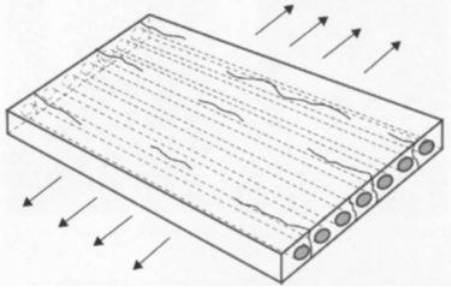

Figure 2.3. Matrix cracking (Milne, 2003)

Separation of adjacent plies in laminates is known as delamination. It results in significant loss in mechanical toughness and load carrying capabilities. Occurrence of delamination can be simulated by having two laminas having different fiber orientations. Loading the laminate in the axial direction will cause the separate plies to experience different stress levels. The difference in stress will give rise to shear stress at the interface and will cause the plies to separate. Laminates that have "hot spots" where there are stress concentration and discontinuous geometries are more susceptible to delamination. Delamination in woven materials subjected to axial loading is minimal compared to the other failure modes. The interface in woven material would be considered discontinuous and therefore resist separation. Figure 2.4 shows delamination in a laminate.

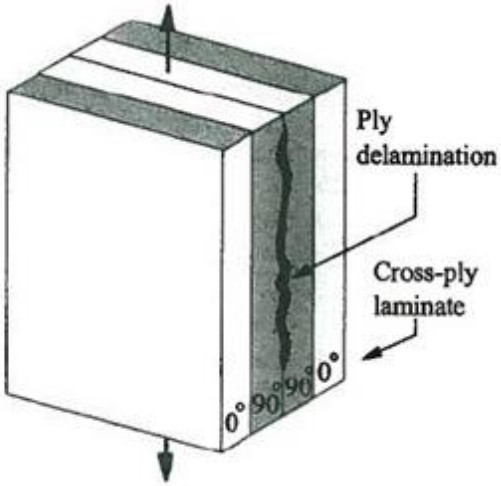

Figure 2.4. Delamination in crossply laminate (K.L. Reifsnider & Case, 2002)

2.3 Damage Evolution in Composites

The failure process of fiber reinforced composites begins when one or more microcracks form within the polymeric matrix (Tuttle, 2004). As mentioned earlier, imperfections may contribute to the formation of the microcracks when the material is loaded. The coalescence of microcracking leads to nonlinear deformation similar to yielding in metallic material, known as formation of a knee in the stress-strain curve of a composite material. The knee for a glass fiber composite can be seen clearly in Figure 2.5. The highlighted portion shows the point where the curve where becomes nonlinear leading to a change in slope. Bulk matrix cracking will occur within this region and will lead to a reduction in stiffness, depending on the material layup. Beyond this region, the fiber is exclusively responsible for the strength of the material therefore the curve exhibits linearity up until failure. Matrix crack growth at lower strains levels propagate shorter distances than those that may occur at higher strain levels due to lower stored strain energy (Johnson A. C., 2012). The direction of matrix cracking in fiber composites is dependent on fiber direction and is parallel to fiber direction (Tuttle, 2004).

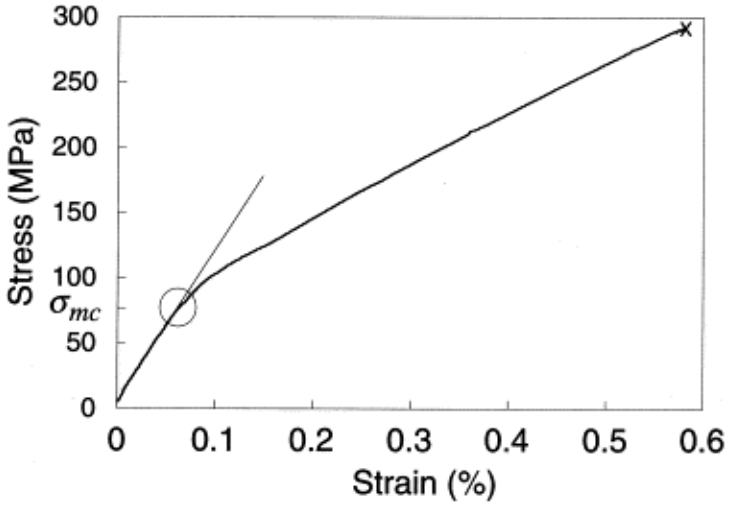

Figure 2.5. Stress-strain curve for glass-epoxy composite (Lara-Curzio, 1998)

With microcracking or matrix cracking signaling the initiation of failure, subsequent failure modes will occur if the loading conditions, load and/or number of cycles, of the material increase. Microcracks grow through the thickness of the matrix until they encounter fibers. The presence of the matrix crack creates a discontinuity which leads to a stress concentration and if the bond strength of the fiber-matrix interface is weaker than this stress concentration, the matrix crack begins to grow parallel along the fiber direction.

Crack growth within a single ply at the fiber-matrix interface, called the interphase region, leads to fiber-matrix debonding. The interphase region plays an important role in the mechanical coupling of the fibers and matrix and contributes significantly to the durability and damage tolerance of the material. It is possible that fiber-matrix separation may be helpful for the composite material in that it helps control the growth of damage of another damage mode, such as intra-ply delamination, and can possibly delay catastrophic failure (K.L. Reifsnider & Case, 2002). Figure 2.6 shows the interaction of several failure modes.

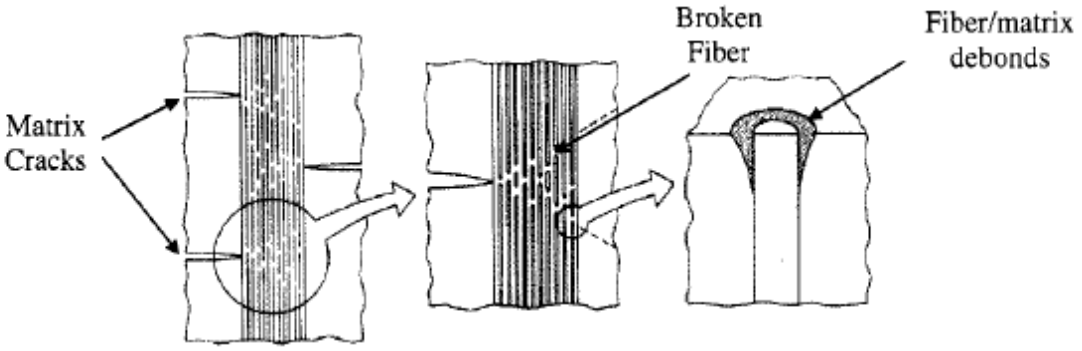

Figure 2.6. Interaction of different failure modes (K.L. Reifsnider & Case, 2002)

One of the primary failure mode associated with unidirectional composites, is fiber breakage. Composite materials are designed so that the overall strength is determined by the strength of the fibers. When the fiber fails, the crack occurs across the diameter of the fiber along a plane that is perpendicular to the fiber direction (Tuttle, 2004). The strength of the individual

fibers is not identical but has a distributed range. Weaker random fibers break at low strains due to imperfections and cause a redistribution of stress into neighboring fibers leading to localized stress concentrations. Such conditions push these fibers beyond their load carrying capabilities and cause simultaneous failure. As the material gets closer to failure, the fibers begin to break in groups, called multi-plets. This is characterized as an exponential increase in the number of breaks that begin around 70% of the ultimate stress of a unidirectional and cross-ply laminate, Figure 2.7.

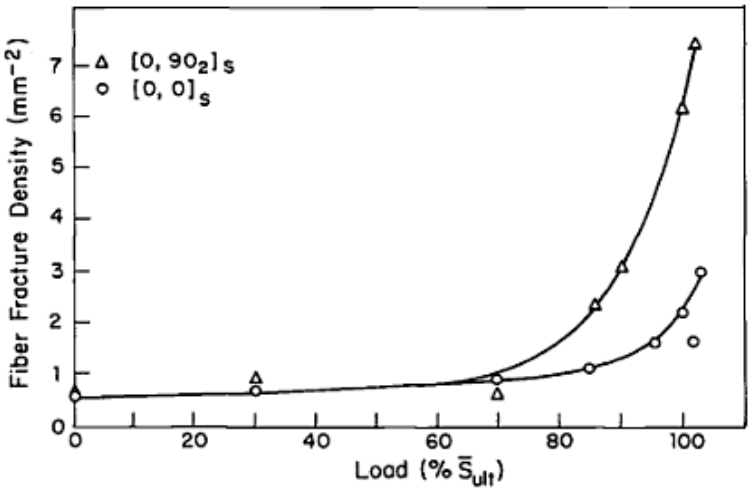

Figure 2.7. Fiber breakage density (K. L. Reifsnider & Jamison, 1982)

Delamination is the other primary failure mode and plays a significant role in the reduction of the stiffness of the material. Delamination growth that occurs within a single ply is known as intraply delamination while crack growth between two adjacent plies is referred to as being interlaminar. As a matrix failure grows along a fiber, delamination is initiated, Figure 2.8. Most commonly, this initiation often occurs at the free edges due to a mismatch in material properties, such as Poisson ratios, of adjacent plies having different orientations. The edges deform differently, causing an increase in interlaminar stress, and when this stress exceeds the bond strength of the plies, crack growth between the plies occur with the amount of strain energy

released during the separation process. Multi-angle composites will experience much more delamination during failure than unidirectional composites.

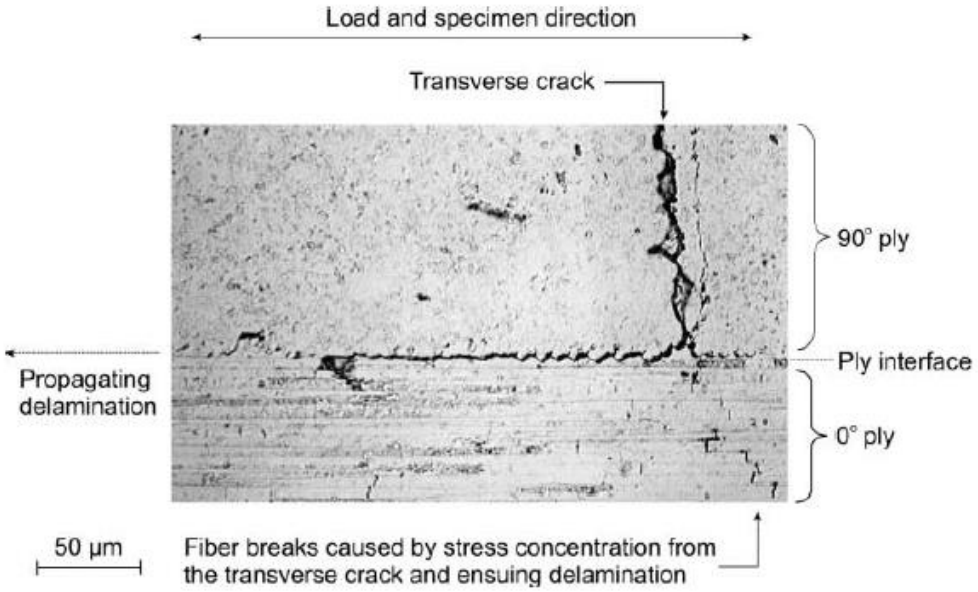

Figure 2.8. Transverse matrix crack and delamination (Gamstedt & Sjogren, 2002)

The presence of multiply damage/failure modes in composites and the interaction of these modes makes the failure process very complex. Failure of the material will occur in stages, as seen in Figure 2.9. The first stage includes the initiation and growth of microcracks and the onset of delamination. There is a steady increase in the amount of damage seen in this region but the amount of damage experienced depends on the layup. While there is minimal damage growth, delamination growth occurs within the second region. This region may also see a significant amount of fiber-matrix debonding. The third stage is characterized by a significant number of fiber failures that leads to sudden fracture of the material.

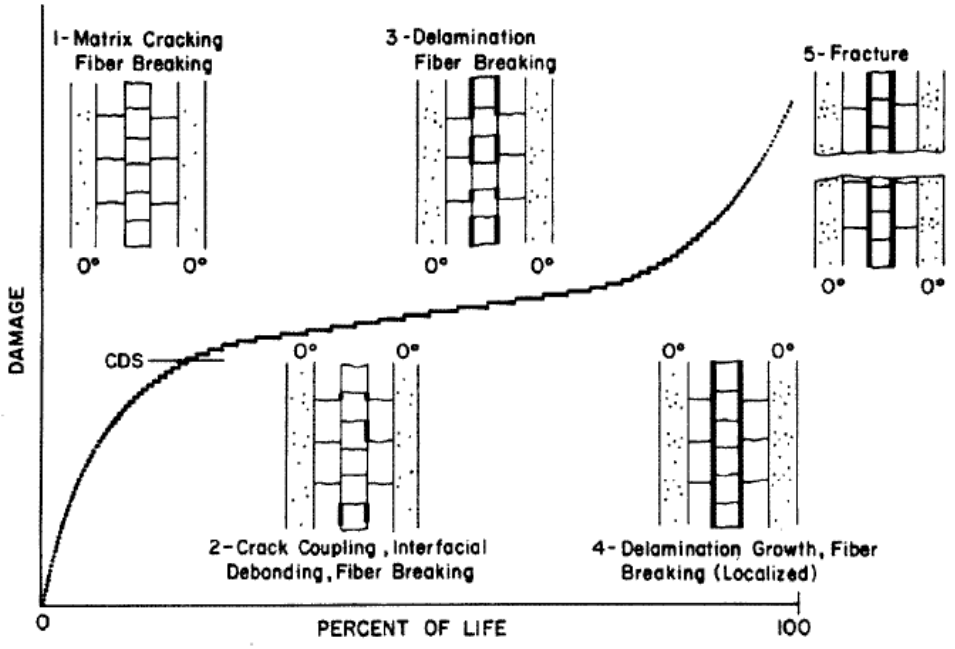

Figure 2.9. Failure process in composite material (K.L. Reifsnider & Case, 2002)

2.4 Wave Propagation

As mentioned earlier, the strain energy released during damage growth is known as an acoustic emission and can be measured as elastic waves. Sources of AE activity can range from friction between surfaces to crack growth for metallic components. Composites are profuse emitter of AE signals and these signals can be generated by different failure mechanisms. The advantages of AE techniques are: high sensitivity, early and rapid detection, real time monitoring, and minimization of downtime for inspection .

An inherent feature of acoustic emissions is that the signals contain information about the source type. The amplitude or frequency content will vary depending on where or how the signal was generated. These signatures can tell whether the source is a surface crack or internal. Signatures can be tracked and as they change over time the type of damage occurring can possibly be extracted. As in composites, a change in signal characteristics may be indicative of a

major failure mechanism occurring. The different failure modes correspond to the level of damage the material has experienced.

To apply AE technique, a good understanding of wave propagation physics is needed. Failure to truly understand the mechanisms governing particle motion could lead to misinterpretation of AE signals. Previous research has found that there are several types of waves. Three types of waves are:

- Longitudinal wave
- Transverse wave
- Longitudinal wave
- Rayleigh wave

The mode of propagation of the different listed about waves can be seen in Figure 2.10. Longitudinal (compression) waves generated particle motion that is parallel to the direction of wave propagation and have the fastest velocity of the known waves. Transverse waves have particle motion that is perpendicular to wave propagation direction. These types of waves are also known as shear waves. There is also a third type of wave know as Rayleigh waves which are surface waves.

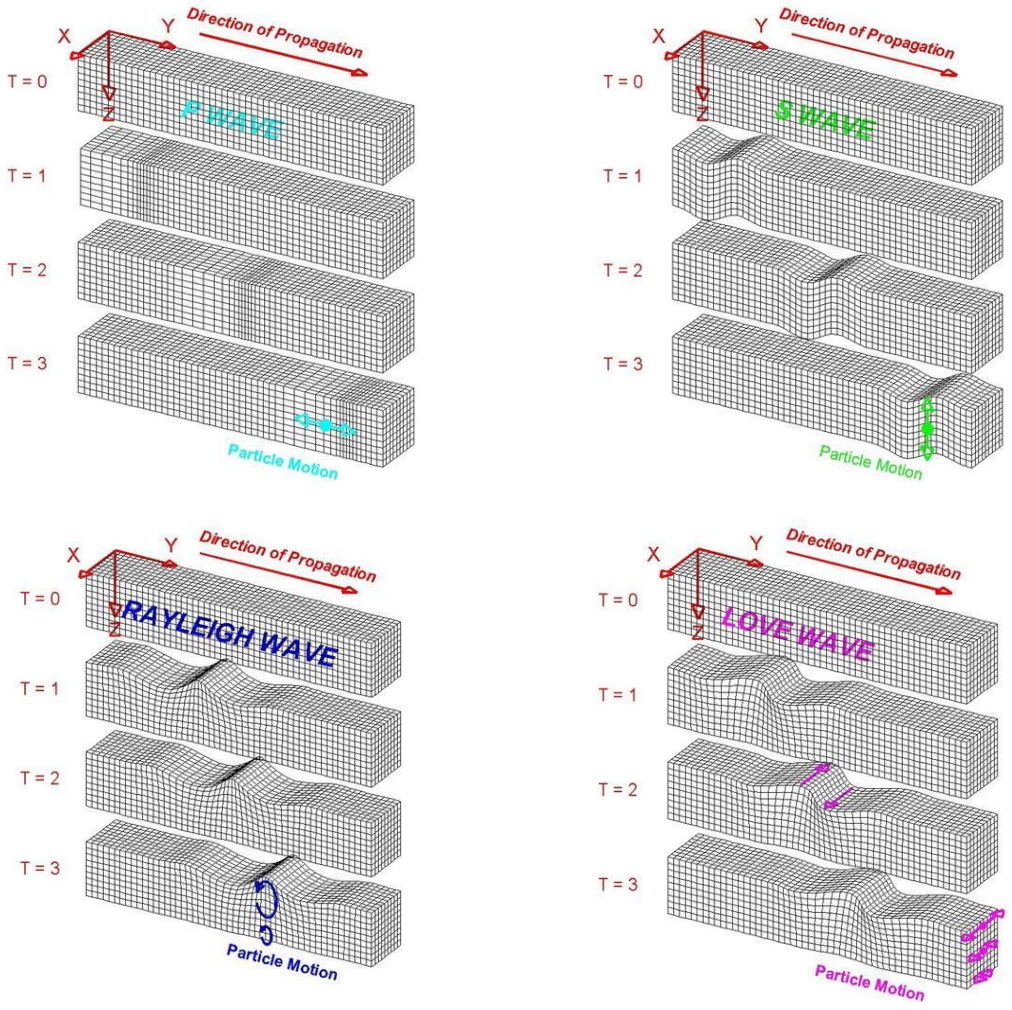

Figure 2.10. Particle displacement and wave propagation in different types of waves (http://web.ics.purdue.edu/~braile/edumod/slinky/slinky.htm)

Elastic waves are governed by the boundaries in which they propagate. When stress waves are generated in thin plates, Lamb waves arise and propagate. These types of waves form when an initial wave interacts with the plate boundaries. As the wave travels, the individual frequency components separate due to varying velocities which is known as dispersion. Dispersion and mode conversion cause the internal waves construct and destruct to form unique patterns of displacement. Depending on how the initial wave was generate, both longitudinal and

transverse particle displacement may be present. Lamb waves are frequency dependent and can be very useful in NDE testing. Some frequencies may be sensitive to a certain type of damage and may show up in the Lamb wave signatures.

The particle displacement of Lamb waves can be symmetric or anti-symmetric with respect to the mid plate of the plate. The symmetric or S_o mode has a higher velocity and contains higher frequencies while relatively lower frequencies tend to dominate the antisymmetric or A_o mode. The propagation velocity of these modes depends on frequency, wavelength, and the material properties. These modes are shown Figure 2.11.

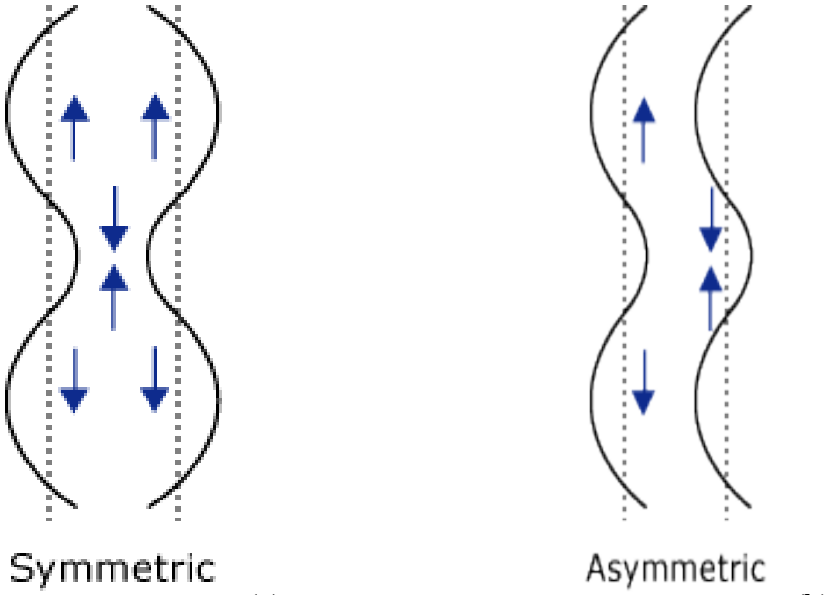

(a) (b)

Figure 2.11. Symmetric (a) and antisymmetric (b) modes

(http://www.ndt-ed.org/EducationResources/CommunityCollege/Ultrasonics)

Other aspects to consider in the study of wave propagation are phase velocity, group velocity, wave scattering, and reflections. The two Lamb wave modes are affected differently by these factors as they propagate within a material. Phase velocity is the velocity at which the phase of the wave propagates in space. In contrast, the group velocity refers to rate at which the

envelope of the whole wave travels in space, Figure 2.12. The term group is given to describe the fact the propagating wave is composed of several individual waves of similar frequency.

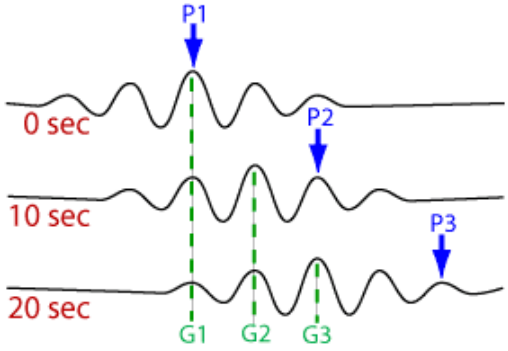

Figure 2.12. Phase vs. group velocity (www.muravin.com)

As the wave advances in space, it encounters the boundaries and reflections occur. Since the Lamb wave modes, either symmetric or antisymmetric, travel at different velocities, reflection of the faster mode may affect measurement of the second mode. The phase of the wave will also change it reflects. If the wave is composed of multiple frequency components, dispersion will happen due to the different velocities of each component. A key parameter in dispersion is the ratio of the thickness of the plate to the wavelength of the component. Dispersion curves depict the velocities of symmetric and antisymmetric modes, starting with the zero-order modes, as a function of the thickness of the plate multiplied by a given frequency, Figure 2.13. The higher-order modes are seen at higher frequency and contain a "cut-off frequency", unlike the zero-order modes. Interactions with changes in geometry, delamination, cracks may also give rise to higher-order modes.

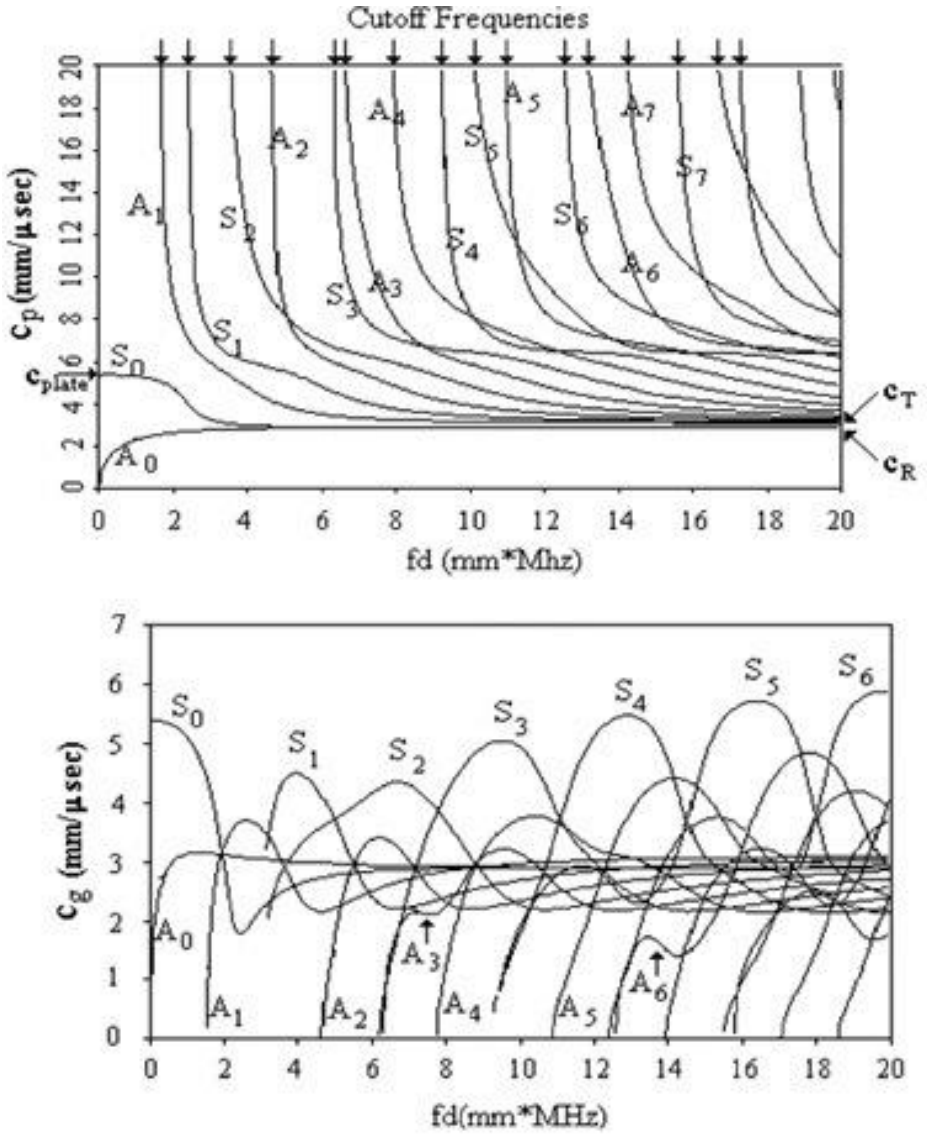

Figure 2.13. Dispersion curves for an aluminum plate (Rose, 2004)

Scattering may happen as a wave travels in heterogeneous material such as composites. The wave encounters the fibers and layers of the composites and begins to break down. Also, as the wave propagates throughout a plate, the amplitude will decrease with distance due to geometric spreading and material damping. These factors contribute to attenuation of AE signals and are more prominent in composite materials. The viscous matrix material used in composite absorbs a significant amount of the strain energy generated during crack growth. Also, some materials may be anisotropic and will attenuate signals differently in various directions.

Anisotropy puts emphasis on the need to accurately locate the source of AE events because the waveform from a given event may look different depending on where the sensor is located.

Many factors can affect AE signals as mentioned above but measurement of such signals is the most critical aspect. Sensor attachment and validation are important when measuring AE signal and much care needs to be taken when bonding. Laser vibrometry can be used to measure absolute out of plane displacement and is a great tool to validate sensor data.

AE signals are produced when a defect grows which makes AE ideal for monitoring dynamic growth in real time. Static damage or damage that is not growing will not produce any emissions. The signals resulting from crack growth in metals can be quite different from what is seen in composites. A single crack may be the driving failure mechanism in metals but several mechanisms will drive failure in composites. A comprehensive understanding of how the mechanisms of AE signals change with material is needed. Several factors that should be addressed:

- Dependable sensor attachment
- Sufficient number of sensors
- Acquisition setup

As mentioned above, composite materials or more specifically CFRPs can be anisotropic and have varying material properties with directions. This can greatly affect the measurement of AE signals and their interpretation. Anisotropy is caused by the non-uniformity of different constituents used in the material. The orientation of fibers, viscous nature of the matrix material, and the laminate layup will alter the original signal. Attenuation and other factors will need to be accounted for when analyzing AE signals in CFRPs.

2.5 AE signal characteristics

Acoustic emission (AE) can be defined as the sudden release of strain energy in the form of stress waves. The stress waves generate vibrations on the surface and within the structure. These stress waves can be measured using various sensors such as: conventional AE sensors, PZT wafer sensors, or laser vibrometry. Primarily, AE signals are generated by incremental crack growth, from both sub-critical and critical sizes. There are several characteristics that make up an acoustic emission signal. A typical AE waveform can be seen below in Figure 2.14 showing each parameter. Acoustic emission waveforms can be described in terms of these parameters for the interpretation and analysis.

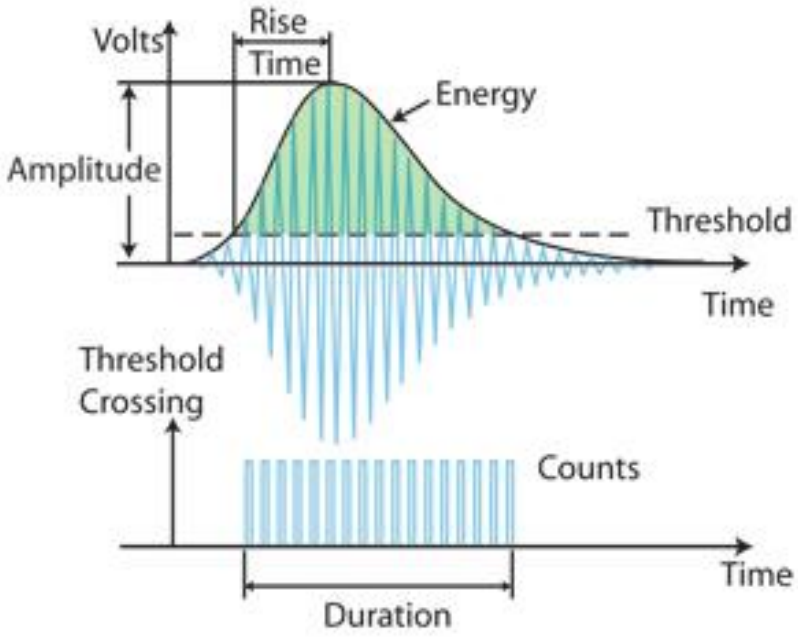

Figure 2.14. Typical AE waveform

(http://www.mistrasgroup.com/products/technologies/acousticemission.aspx)

Hit – a single signal resulting from defect growth

Peak amplitude (amplitude) – maximum absolute value point of an AE waveform

Threshold – minimum amplitude level of a signal that will be measurement

Time of hit – time corresponding to when the threshold is crossed

Counts – number of times the threshold is crossed by a single signal

Duration – the time between the initial threshold crossing and the last crossing

Rise time – the time between the initial threshold crossing and the peak amplitude

Average frequency – the number of peaks within a given duration

Peak frequency – the maximum frequency reading in the power spectrum of the signal

Energy – integral of the rectified voltage over the duration of the acoustic emission hit or the area below the curve enclosing the waveform

2.6 Acoustic Emissions and Composite Materials

The above features are dependent on material geometry, material properties, sensor performance, and acquisition system capabilities. Most research that uses AE techniques monitor certain parameters over time and attempt to relate changes in the parameters to defect growth. A solid understanding of the various aspects of AE signals has led to more sophisticated analyses that involve database training and pattern recognition. Stand-alone technology or systems that require minimal human interaction could be developed from such research. These approaches can lead to more accurate assessment of damage and prediction of structural integrity.

There are several failure modes seen in composite materials, as mentioned earlier. Each failure mechanism should generate a distinct signal and unique characteristics, such as the parameters mentioned above. Some researchers have attempted discriminate the different failure mechanisms by monitoring the various AE parameters. It was found that the different failure modes occupy unique frequency ranges (Jong, 2005).

Acoustic emission can be used to determine the mechanical properties of sandwich composites under mode I delamination (Hajikhani, 2011). A parameter, Sentry Function, was developed and utilized to estimate the fracture toughness of the sandwich laminates. The frequency domain of AE data was used to discriminate between the different failure modes seen during DCB testing of glass fiber composites (Arumugam, 2011). The frequency content was extracted using a Fast Fourier Transform (FFT) and the frequency range of each mode was noticed. Acoustic emission signals of each mode could be isolated by examining the frequency range of the signals. One researcher estimated the critical energy release rate of cryogenic fracture in CFRP woven laminates using numerical simulations (Kumagai & Shindo, 2004). The cumulative AE energy was related to onset of microcracking. Quasi-static loading of this material was done to initiate damage growth. AE was also used to predict the residual fatigue life of ceramix matrix composites (Momon, 2010). The elastic energy released was seen to accelerate before final failure. A coefficient of emission was calculated and used to monitor damage growth resulting from constant loading.

Two of the primary damage mechanisms were tracked in unidirectional composite lamina: matrix-cracking and fiber-matrix debonding using acoustic emission (Bocchhieri, 2004). The focus was to see if matrix crack signals varied with fiber direction. Using a loading parameter, the damage state was determined. Another researcher studied acoustic emission in wide composite specimens by modeling elastic wave propagation in plates (Scholey, 2006). A frequency domain propagation transfer function was developed to account for beam spreading, excitability, time-delay and attenuation. The properties of Lamb wave propagation were predicted with very little experimental knowledge. Some researchers conducted mode I and mode II delamination testing and monitored the AE parameters (Aggelis, Barkoula, Matikas, &

Paipetis, 2010). The increase in the signal amplitude was associated with delamination, which concentrated the energy of the acoustic emission near the surface. Another group used AE to track the progression of damage in composites under quasi-static loading (Bussiba, Kupiec, Ifergane, Piat, & Böhlke, 2008). Traditional parameters such as counts and amplitude were used to track damage.

2.7 AE resulting from Static and Fatigue Loading

The static and fatigue strength of composites determines whether the material is suitable for certain loading environments. While some materials have high static strength, they may not be sufficiently flexible and will fail when experiencing varying loading cycles. Such brittle materials can range from concrete to ceramic. Quasi-static loading is commonly used to determine the ultimate strength of a material in a relatively short period of time.

Testing of static or quasi-static specimens was done in accordance to the ASTM standard, which determines the in-plane tensile properties of high modulus reinforced polymer matrix composites under uniaxial tensile loading (D3039, 2013). There are guidelines for recommended specimen and tab dimensions as well. The strain rate chosen should produce failure within 1 to 10 min or a displacement rate of displacement rate of 2 mm/min. Fatigue testing follows the standard which defines the fatigue behavior of polymer matrix composite materials subjected to tensile cyclic loading (D3479, 2013). The dimensions of fatigue specimens are the same as static specimens. Loading, however, is varied and defined as a percentage of the ultimate stress and involves a loading ratio. Cycles to failure is a function of these loading parameters.

According to one researcher, fiber failure is based on the fact that the strength of the fiber is not constant along the length (Daniel, 1994). In addition, not all fibers fail at once, but single fiber breaks occur at weak spots. The localized stress state around the fiber gives rise to

interfacial shear stress, which causes fiber debonding. Failure due to static loading is normally depicted using a stress-strain curve.

Fatigue loading on the other hand, is a much longer process and dependent on the loading parameters. It is important to understand fatigue failure when characterizing composites. Another approach used the fracture mechanics model to describe the behavior of an initial crack under stress (Evans, 1974). The crack propagation rate was under cyclic loading was determined using slow crack growth parameters.

Much research has been done to predict the fatigue life of CFRPs. A delayed-fracture model was used for transverse cracking in CFRP cross-ply laminates under static fatigue loading (Ogi, Yashiro, Takahashi, & Ogihara, 2009). First, a delayed fracture model was established based on the slow crack growth (SCG) concept. Second, a probabilistic model was applied to transverse cracking. Results of the reproduced transverse crack density at various applied loads agreed well with the experimental data.

As mentioned earlier, the fatigue failure process of composites can be complex and must be well understood when classifying damage. One such research focused on characterizing the fatigue crack growth of off-axis plies in quasi-isotropic GFRP laminates under constant amplitude fatigue loading (Huang, 2002). Monitoring of the individual fatigue cracks reveals three distinct stages of crack growth:

- Initiation
- Steady-state crack growth
- Crack interaction and saturation

Finite element simulations have been used to model the stress redistribution due to matrix cracking and stiffness reduction. It was found that strain energy release rate associated with

matrix cracking correlated to fatigue crack growth. Some evaluated the stiffness and dissipated energy per cycle to characterize damage in GFRC laminates (Giancane, Panella, & Dattoma, 2010). These two parameters are shown to be related to the damage state of the material and are used for predicting the remaining life. Three distinct regions of the failure process were also noticed.

A stiffness-based model to characterize the progressive fatigue damage in quasi-isotropic CFRP composite was done by (Ahmadzadeh, Shirazi, & Varvani-Farahani, 2011). The damage model was also based on three regions of damage and measures the accumulation of failure in the separate plies. Fatigue data from experiments fit between the predicted damage curves of 90°, 0° and ±45°. The effect of stacking sequence was also assessed and it was found that the model recognized the changes in the failure mechanisms resulting from fatigue failure.

Transverse cracking in GFRP cross-ply laminates subjected to uniaxial fatigue loading has also been studied (Berthelot, 2003). Finite element modeling was used to evaluate the stress field when there is progressive cracking across the width of the specimen. It also shows that the shearing through the thickness of the 0° layers is related to changes in stress field.

One researcher developed life curves for transverse crack initiation, delamination initiation, and final failure for cross-ply and multi-directional GFRP laminates (Wharmby, 2003). Failure due to transverse cracking was showcased using a linear relationship between the normalized stiffness and crack density. The interaction of the different failure modes was also examined.

Others examined the development of fracture paths in CFRPs as damage progresses (K. Reifsnider & Majumdar, 2011). The local stress concentration at each fiber break determines whether the damage grows beyond the fiber. Furthermore, the fracture path was controlled by the

statistical accumulation of fiber fractures. Impedance spectroscopy was used to monitor the accumulation of internal micro-fractures in terms of final failure.

A CFRP laminate with a circular hole under in-plane uniaxial loading has been studied as well (Satapathy, 2013). An analytical model based on minimum strength and fiber failure criterion was used to evaluate the fatigue behavior. The model considered degradation of material strength as a function of applied number cycles. Using ply-by-ply analysis, the number of cycles to failure and the location of failure could be determined. Another group investigated the effect of size on tensile strength of composite material with circular holes (Hallett, Green, Jiang, & Wisnom, 2009). Delamination initiated around the hole edge then linked together around. The distance for the delamination to link up was shorter for the smaller diameters, thus the failure stress was higher for smaller diameters due to localized damage relieving stress in this region.

In summary, the literature reviewed dealt with studying the initiation of damage in composite materials, using finite element modeling to simulate failure evolution, and validation of models through experimentation.

2.8 Fiber optic strain measurement using Fiber Bragg gratings

As damage progresses in a structure, the global effect can be seen in terms of strain distribution. Localized damage can propagate if the critical load level continues to be applied. While sensors can measure the AE signals resulting from damage growth, they are unable to directly give an assessment of the structure's integrity. Various strain gages and extensometers are able to measure strain but can only do so on a point-by-point basis. Fiber optic sensors, on the other hand, can monitor large areas with minimal instrumentation. This research will utilize

uniform Fiber Bragg gratings (FBG) sensors to measure the strain distribution in CFRP laminates as damage occurs.

Fiber Bragg grating is a type of optical sensor used to measure strain. FBGs are created by laser etching of particular points along a glass fiber. These regions are etched in a periodic variation altering the refractive index and are designed to reflect light at a certain wavelength. Thus, any change in wavelength relative this designed wavelength can directly be attributed to the occurrence of strain. A broadband reflector is used to create interferometry. Figure 2.15 shows the methodology behind FBG strain measurement.

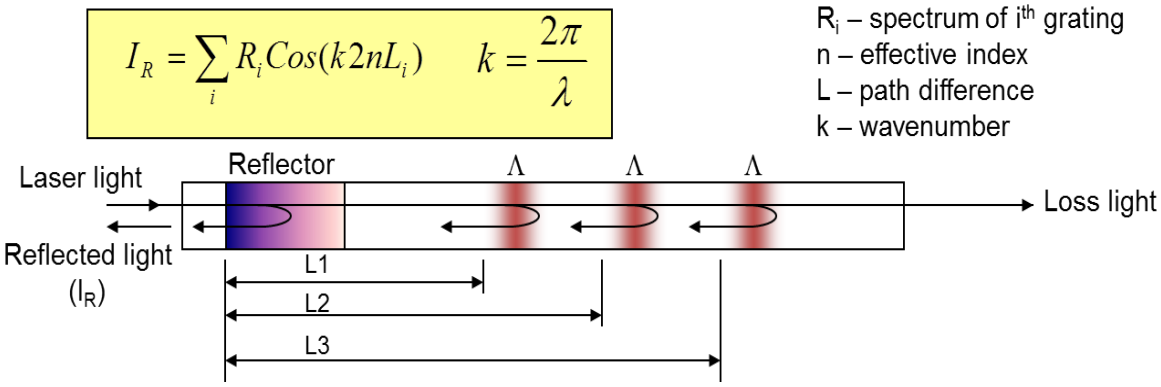

Figure 2.15. Fiber Bragg grating strain measurement technique, *NASA-Dryden*

The wavelength at which the gratings are written is called the Bragg wavelength (λ_B), seen in Figure 2.16.

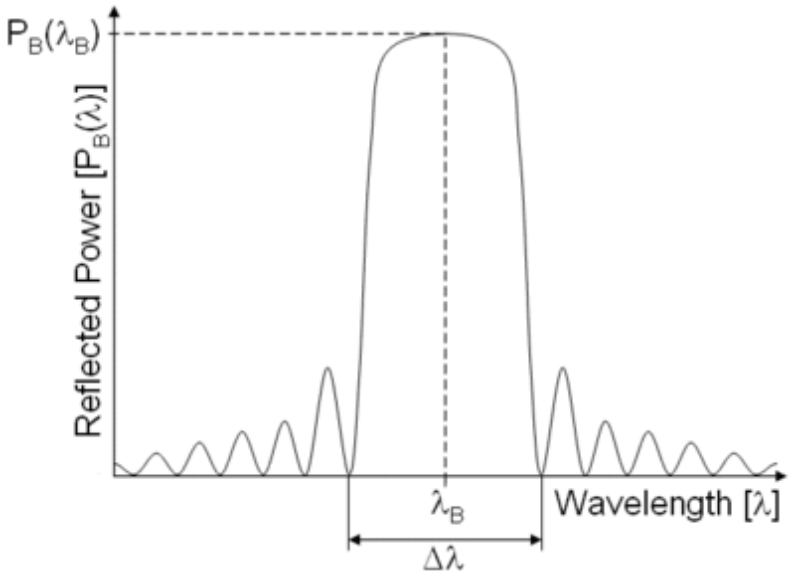

Figure 2.16. Bragg wavelength (http://en.wikipedia.org/wiki/Fiber_Bragg_grating)

As mentioned above, a shift in the wavelength experienced by each grating corresponds to strain. The following equation is used to calculate strain:

$$\frac{\Delta\Lambda}{\lambda} = k\varepsilon$$

where $\Delta\Lambda$ is the shift in wavelength (negative = compression, positive = tension), λ is the Bragg wavelength, ε is strain, and *k* is the gage constant

FBG sensors have the ability to monitor strain over a large area. Damage in composites from impacts can propagate without being visibly noticed. When load is applied to structure, the damaged area will cause a redistribution of stress that shows up as changes in the localized strain fields. Fiber optic sensors can be used to measure these changes. FBG sensors have many advantages over traditional strain measurement devices and several are mentioned below:

- Immune to electromagnetic / radio-frequency interference and radiation
- Lightweight fiber-optic sensing approach having the potential of embedment into structures
- Multiplex 100s of sensors onto one optical fiber

- Uniform gratings are written at the same wavelength
- Uses a narrowband wavelength tunable laser source to interrogate sensors
- Typically easier to install than conventional strain sensors

Table 2.2.

Various fiber optic sensors (Fidanboylu, 2009)

Type of fiber optic sensor	Description
Intensity-based	Relies on change in signal amplitude
Wavelength modulated	Uses changes in wavelength for measurement (FBG)
Phase modulated	Uses changes in phase for detection (Mach-Zender, Michelson, Fabry-Perot, Sagnac)
Polarization modulated	The direction of the electric field portion of light is used for measurement

Fiber optic research has been focused on a broad range of subjects; from quality assurance to geological studies to health monitoring of civil and aerospace structures. The quality of embedded or surface bonded fiber sensors has also been studied (Shiuh-Chuan, 2009). The bonding characteristics, such as protective coating, layer of adhesive, and the length of bonding, play a key role in the transfer of strain from the host material to the fiber. Analytical and finite element modeling were used to predict the strain transfer into the fiber. A parametric study showed a long bonding length and high modulus of protective coating would increase the percentage of strain transfer. A Mach-Zender interferometer was used to measure the strain levels of the fiber.

A comparison FBG sensors to conventional electrical strain gages has been an area of focus also (Kleckers, 2007). The long term reliability of each was tested by applying a cyclic strain of ±1000μm/m. The measurement characteristics of the optical fiber did not change after

10^7 cycles. In contrast, an irreversible change in zero was noticed in the electrical strain gages. This work agreed with previous work that concluded that FBG sensors are not affected by fatigue strain of ±2000 μm/m.

Another research group conducted laboratory tests to obtain the relational expression computed from the interrelationship of the variation in the Bragg wavelength, temperature, and displacement (Sanada, Sugita, & Kashiwai, 2012). A muli-interval displacement FBG sensor was used to monitor the short and long-term rock mass behavior. The results of laboratory evaluated the accuracy to be better than +/-0.5% of the measurement range. Also, it was shown that the displacement values from the fiber optic sensor and a conventional extensometer were almost equivalent. An advantage of the fiber sensor was the insusceptibility to noise.

Civil structures have been involved in much of fiber optic research. One researcher proposed a continuous fiber optic based monitoring system on pipelines in nuclear power plants (Yang, 2012). Guided waves were produced by the system and measured using fiber optic cables. The fiber was split with one being used to actuate a macro fiber composite (MFC) transducer and the other is used as FBG sensors to measure the response. The MFC was attached along the circumferential direction of the pipe and excite the longitudinal and flexural modes, which were measured by the FBG sensors. Guided waves will interact with defect and will alter the original signal. Finally, using data from initial pitch-catch tests, a damage sensitive feature was extracted from the measured response.

Monitoring the integrity of bridges has become an importance topic. One researcher looked at the long term monitoring of the Leziria Bridge in Portugal (Sousa, 2011). The fiber optic system was designed to survey the structural condition and provides real-time monitoring by assessing several factors: structural information, durability data, and environmental

parameters. The main focus was to present a long-term monitoring solution for the bridge. Another researcher used fiber optics to evaluate the structural health of stay cables, which are a critical component of bridges (Li, Ou, & Zhou, 2009). They are known to suffer from effects of fatigue and corrosion. In this case, fiber optic sensors were attached to the cables and the stretching of the cables due to loading were recorded and assessed.

Some applied FBG sensors for assessing the health of an adaptive wing (Mieloszyk, Skarbek, Krawczuk, Ostachowicz, & Zak, 2011). The wing's shape can be controlled and altered using shape memory alloy (SMA) actuators. First, the response of the wing was simulated using finite element modeling using ABAQUS and compared to strain values measured by FBG sensors during testing. The results were used to determine the moment at which each SMA actuates.

Others used both conventional AE sensors and FBG sensors for damage detection (Raju, Azmi, & Prusty, 2012). The failure of composite top-hat stiffeners was characterized and quantified. A significant difference in the conventional parameters (amplitude, duration, energy released, counts, etc.) was seen for the different failure modes. However, analysis of the waveforms only allows two failure modes to be distinguished: crack propagation and delamination.

In summary, the application for fiber optic technology covers a broad array of fields. The many advantages and versatility of this technology has fueled this growth. A primary focus for fiber optics has been strain-based measurements but advancements are leading to ultra-sonic measurement systems. In many cases, a conventional strain gage was used to validate the strain data. A combination of different sensing technology could possibly provide a more reliable and dependable structural health monitoring system.

2.9 Pattern recognition and AE

As the ability to distinguish the different failure modes grows, characterization and quantifying of each will become more accurate. The next step is to develop a methodology to automate the discrimination of the different mechanisms. This is ultimately called pattern recognition and some previous work regarding classification of AE signals are discussed below.

A neural network was used to train a database and utilized correlation to isolate the different failure mechanisms (Ativitavas, 2005). A backward propagation method was used to relate a damage signal to it's source and a probabilistic neural network constructed a density function based on training samples of tension test specimens. These tests were primarily glass fiber/resin composites but did involve a carbon/resin and several hybrid/resin specimens. Full scale bending test on beams and several other types of tests were done to simulate damage. Conventional AE parameters were used to discriminate the different failure mechanisms.

Others used two artificial neural networks, Kohonen-self organizing feature map (KSOM) and multi-layer perception (MLP) to analyze AE signals (Bhat, Bhat, & Murthy, 2008). Both fatigue and compression specimens were cut from a unidirectional CFRP. All fatigue tests included three loading periods with each having 150,000 load cycles. Compression tests were done under load control by holding the load for 1 min every 4kN up to 24kN or until failure occurs. The resulting AE signals were clustered using KSOM, which incorporated such information as amplitude distribution, time of occurrence, ultrasonic imaging, and even the design of the laminate. Afterwards, the supervised learning network, MLP, was used to automatically classify the AE signals.

Another group worked on an intelligent system for structural health monitoring that relied on dynamic strain measurements (Loutas, Panopoulou, Roulias, & Kostopoulos, 2012). The

structure used represented a typical aerospace component with a frame, skin and stringers. Damage was simulated by placing mass at several points, which altered local strain fields. Several FBG sensors measured strain data or the dynamic response. Discrete wavelet transforms and support vector machines were the advanced signal processing and pattern recognition techniques used. The damage and it's location were able to be determined.

Unsupervised pattern recognition analyses (fuzzy c-means clustering), which uses principal component analysis, to distinguished the different types of damage was used by another research group (Refahi Oskouei, Heidary, Ahmadi, & Farajpur, 2012). Damage was simulated by DCB testing of C/C composites of different layups. Delamination was represented as bulk failure composed of several sub-failures: matrix cracking, fiber debonding, and fiber breakage. Several time domain methods are included in the classification process to improve the characterization and discrimination of the damage modes. The results show a good fit between clusters and damage modes.

Clustering of AE signals using a k-means algorithm has also been done (Sause, Gribov, Unwin, & Horn, 2012). The amount of separation between each cluster is calculated using several statistics-based methods, such as Davies-Bouldin and Tou indices, Rousseeuw's silhouette, and Hubert's Gamma approach. This methodology automates the evaluation of clusters without previous knowledge about the AE signal. The classification of AE signals was validated using data from failure loading of CFRP specimens.

2.10 Summary

The application of AE techniques for structural health monitoring was discussed in this chapter. Most research focused on identifying damage in terms of the different failure modes: matrix cracking, fiber pullout, fiber breakage, and delamination. Critical components of

aerospace as well as civil structures have been the primary focus of AE experimentation. The incorporation fiber optic technology has revolutionized health monitoring techniques and more sophisticated pattern recognition methodologies offer real-time assessment of damage.

CHAPTER 3

AE Instrumentation and Test Materials

3.1 Introduction

The most important component of health monitoring is the sensor used for measurement. AE measurements rely on the type of sensor used and it's orientation with respect to the source. Different damage mechanisms produce unique signals and this chapter deals with the instrumentation used to capture AE signals in CFRP composites. Signal characteristics such as frequency content and mode of propagation are taken into consideration. Also, sensor calibration is discussed. Static and fatigue tests utilized the same experimental setup mentioned in this chapter.

3.2 CFRP Laminates

Five carbon fiber-epoxy laminates (2 cross-ply and 3 quasi-isotropic) of various thicknesses were provided by NASA-Dryden. The plies were stacked, vacuumed bagged and heated 2°F/min to 250°F followed by 1 hr hold at 250°F followed by natural cool down. The first set of tensile specimens was cut from a 2' x 2' orthotropic panel with 12 plies with a $[0/90]_{3S}$ layup. Specimen size was determined by ASTM D3039 tension test standard. A diamond saw was used to cut specimens with dimensions of 11" x 1". A panel of 23 3/8" x 12" was also fabricated from the orthotropic laminate and was used for damage progression testing. For the quasi-isotropic material with a layup of $[+45/90/-45/0]_{2S}$, several specimens of 11" x 1" dimensions and a 21" x 11" panel were cut from one of the laminates.

3.3 AE Instrumentation and Measurement

PZT wafer sensors (Figure 3.1). The sensors used for measurement are PZT sensors, shown in Figure 3.1., which have the dimensions of 20mm x 10mm x 0.5mm. They are used to measure the AE signals accompanying damage in composite specimens and have an advantage over conventional AE sensors, which is being able to capture the characteristics of the lamb wave modes. These PZT sensors are known to have a frequency range of 100 to 700 kHz and are adhesively bonded to specimens.

Figure 3.1. PZT sensors on CFRP specimen

Olympus Ultrasonic and PAC resonant sensors (Figure 3.2). Ultrasonic and PAC resonant sensors were also used in the static and fatigue tests. They were coupled with ultrasonic gel and their primary function was to aid in source identification. These sensors were placed outside of the gage length of the specimens and, using a difference in time of arrival between the PZT and the ultrasonic/PAC sensors, the origin of the signal could be determined. The Olympus ultrasonic sensors have a frequency response of 50 to 5MHz (http://www.olympus-

ims.com/en/ultrasonic-transducers/) while the PAC resonant sensors have a frequency range of 100 – 400 kHz (PCI-2 based AE system manual 2004).

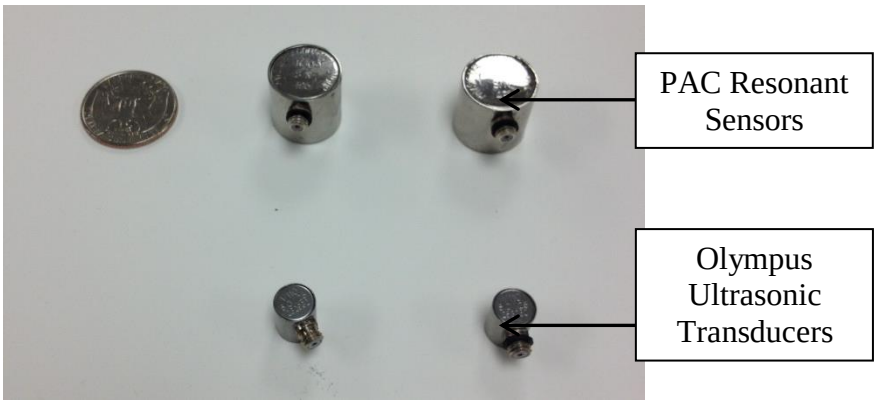

Figure 3.2. AE Transducers

PAC Preamplifiers (Figure 3.3). After AE signals were measured, they were amplified using PAC preamplifiers. There are three setting for such amplifiers: 20dB (10X), 40 dB (100X), and 60dB (1000X). For the tension and fatigue tests, 40 dB gain was used.

Figure 3.3. PAC preamplifiers

PCI-2 Data Acquisition and AEwin3.2 Software (Figure 3.4). A PCI-2 data acquisition system was used to record AE signals. All waveforms were visually displayed using

AEWin 3.2 software, which can record numerous features (amplitude, duration, energy, etc.) of AE events. This software is run on a 32-bit Windows operating system.

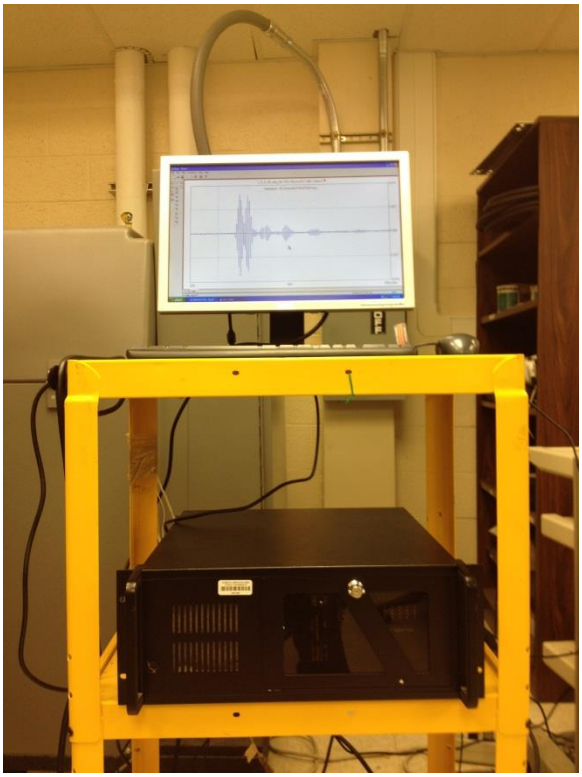

Figure 3.4. PCI-2 data acquisition system

Material Test system (MTS 810). Tension and fatigue tests were carried out using MTS 810 machines. Two machines are used and are capable of applying maximum loads of 20 kips (88 kN) and 50 kips (222 kN). The load applied and displacement of the load heads are recorded using the PCI-2 data acquisition system.

MTS Extensometer (Figure 3.6). For strain measurements of the specimens, an MTS 634.11 Axial Extensometer was used. It is perfectly suited for measuring strain in tension or fatigue tests and has strain range of +20% to -10% (http://www.mts.com/en/products/). Small aluminum tabs were bonded on each side of the gage length and were used to hold the knife edges of the extensometer in place. Rubber bands were used to attach the extensometer to the specimen.

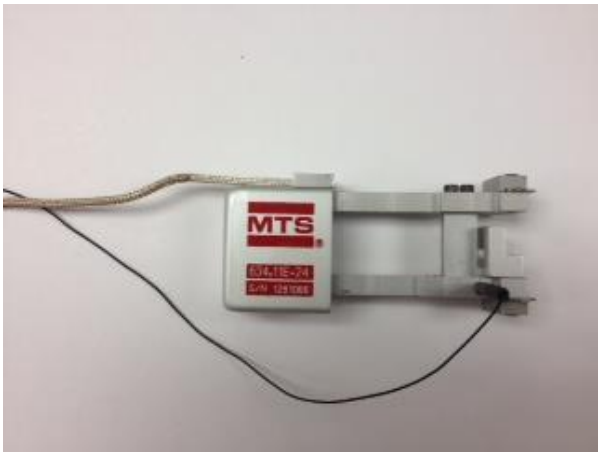

Figure 3.5. MTS extensometer

Fiber Optic Sensors. The fiber optic system uses a wideband tunable laser to interrogate the FBG sensors and has a maximum sampling frequency of about 100 Hz. The fiber optic wire itself has a diameter of ~50μm (250μm with coating and casing) and contains FBG sensors spaced 0.5" apart. A minimum bend radius of 0.5" was used for testing of a glass-epoxy composite panel with a center drilled hole. Strain was measured by 149 FBG sensors during static and fatigue loading, with emphasis on the area where stress concentration occurs.

3.4 Lead break tests

Lead breaks tests are a common practice in AE testing are used to simulate short duration events such as crack growth. The measure signal in response to a lead break event can be used to verify that the sensor is working properly. Each specimen used in testing have bonded PZT wafers on either side of the gage length. Using lead breaks, the response of each sensor was compared to ensure that they both are functioning in the same manner. It should be mentioned that even "identical" sensors will not perform identically. For this research, an amplitude difference of 15-20% between two sensors measuring an event that is equal distance from both would suffice. These tests are modeled after the Hsu-Nielsen Source test and use a 3mm long, 0.5mm diameter lead broken at an angle on the surface. Figure 3.6 shows the typical response of

a PZT sensor after a lead break and the corresponding wavelet. The wavelet transform contains the expected frequency content from the lead break test.

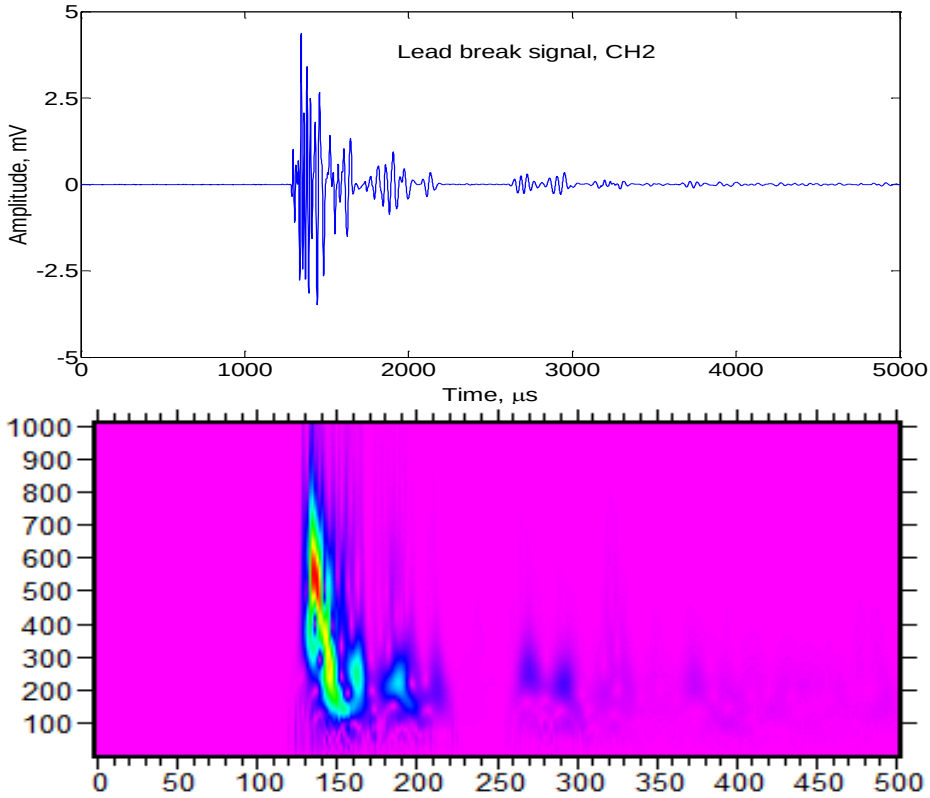

Figure 3.6. AE signals from lead break test and corresponding wavelet

CHAPTER 4

Static and Fatigue Results

4.1 Introduction

Static and fatigue test were done to simulate damage in CFRP composite specimens and the results are presented in this chapter. As mentioned earlier, the damage process in composites happens in different stages and each stage corresponds to a certain failure mechanism. The goal was to initiate and grow damage and measure the resulting AE signals. Unique characteristics, such as frequency content and duration, seen in the signals make it possible to distinguish the failure modes. Part one of this section deals with quasi-static tests while part two discusses fatigue loading. Both quasi-isotropic and cross-ply specimens were tested and the details are described in the following sections.

Tabbing. To prevent damage from gripping of the specimen, tabbing was done according to ASTM standard for tensile testing. A glass fiber composite panel was used to fabricate the tabs, which were recommended to have an orientation 45˚ to the loading direction for compliance purposes. The tabs were 2.5” x 1” x 0.06” with a bevel length 0.5” at an angle between $30-45°$. Quickset epoxy was used to bond the tabs which and was cured for 24 hours under reasonable pressure.

Instrumentation. For sensor attachment, the specimen had to be sanded at the desired sensor locations. Stainless shim stock steel foil of 0.0005” thickness was glued to the specimen at opposite ends of the gage length to increase conductivity. Two PZT wafer sensors were attached to the foil with superglue approximately 3” from each end of the specimen giving a gag length around 5”. The bond was cured for 24 hours and shielded DCB cables were connected to the wafers. The frequency response of the PZT sensors is 100 to 700 kHz and the dimensions are

10mm x 20mm x 0.5mm. A prepared specimen ready for testing can be seen in Figure 4.1. Also, two PAC Micro-30 sensors of 0.25” diameter were attached on the opposite side of the wafer sensors to aid in source identification. The Micro-30 sensors operate between 100 to 600 kHz. Using a difference in time of arrival between the PZT sensors and the ultrasonic sensors, it can be determined when an event occurred within the gage length or at the grips as a result of fiber crushing. An MTS extensometer was used to measure the strain during loading. The Micro-30 and extensometer were removed around 70% of predicted failure to prevent damage to them.

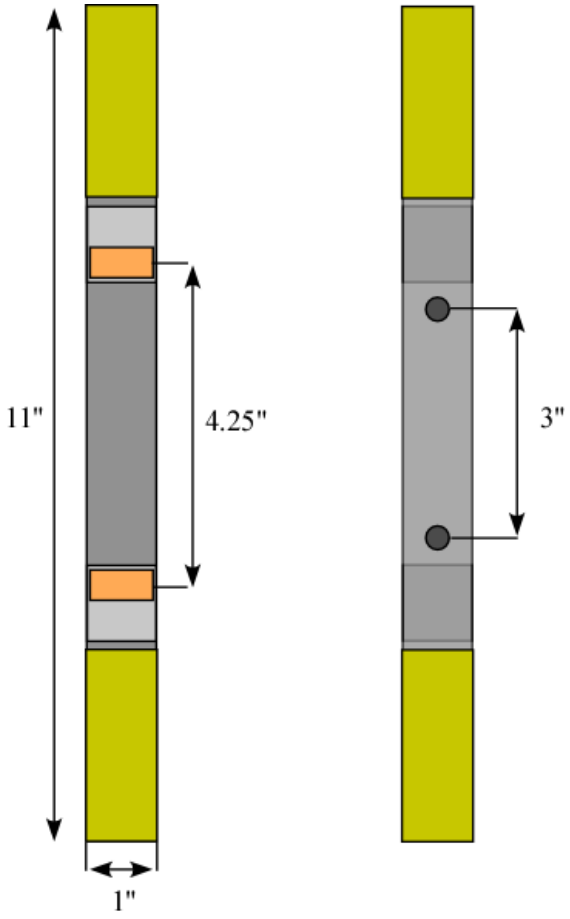

Figure 4.1. Schematic of instrumented tensile specimen: Front (PZT) and back (ultrasonic)

4.2 Testing

4.2.1 Static Tests

After verifying the sensitivity and accuracy of the sensors, the specimens were loaded into the 810 MTS machine and placed under quasi-static loading at a rate of 1.5 kips/min originally. Due to the loading sequence being paused around 70% of predicted failure to remove sensitive equipment, the resulting plots may show an abnormality around this region. Failure occurred around 5-10 mins for the specimens which falls within the standard recommended time for tensile testing. For each static test, the corresponding AE signals and failure load were recorded. Five total static tests were done for each lay-up with failure occurring within the gage length. The test procedure was the same for both cross-ply and quasi-static specimens. Figure 4.2 shows the experiment setup used to acquire AE signals.

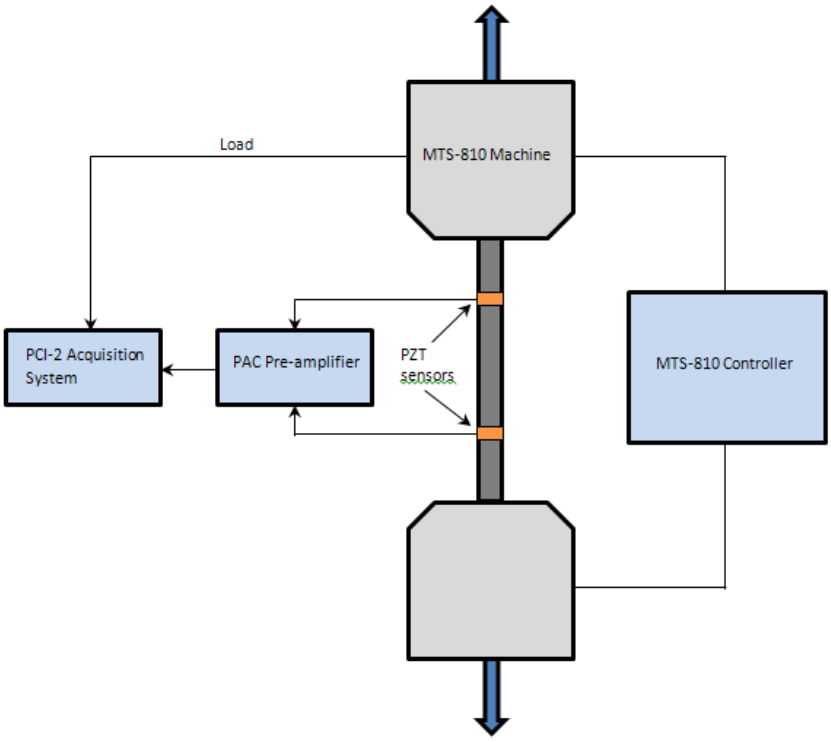

Figure 4.2. Experimental setup for static and fatigue tests

The acquisition parameters were:

Table 4.1.

Acquisition parameters

Threshold	Pre-amp Gain	Frequency Filter	Sampling rate
40 dB	40 dB	100kHz – 1MHz	5 MHz

As mentioned earlier, very large number of AE signals are generated in composite materials. Loading the specimens at the recommended rate generated a very high density of signals for a given time window. This can clearly been seen in a waveform taken during this fast loading sequence, Figure 4.3. In order to decrease the density of the measured signals, the loading sequence was slowed to 10 kips/hr. Using this loading rate caused the failure time to fall well outside the time to failure window given by ASTM-3039 standard for determining in-plane tensile properties but this research is more focused on measuring and analyzing AE signals. Slowing down the loading dramatically increased our ability to measure and accurately process individual AE events. Figure 4.4 shows a tensile specimen with an extensometer attached mounted in the MTS-810 machine.

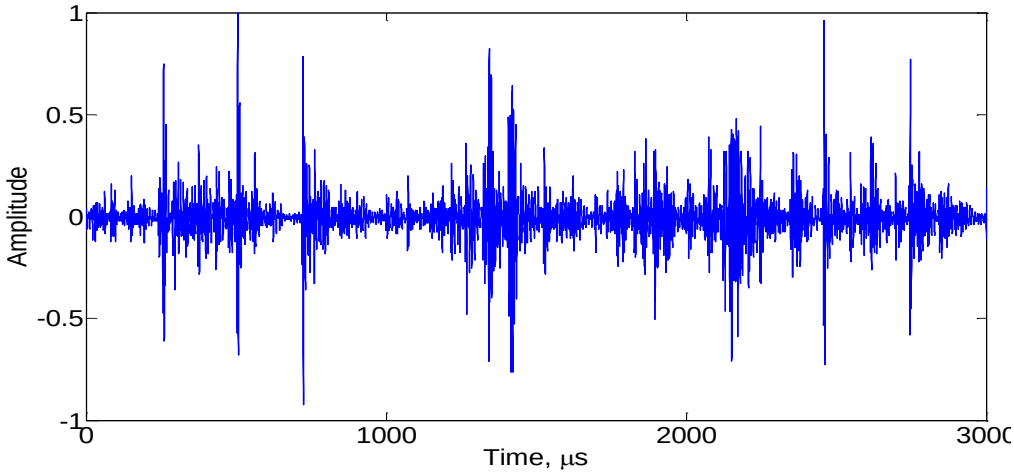

Figure 4.3. Waveform measured during fast loading sequence

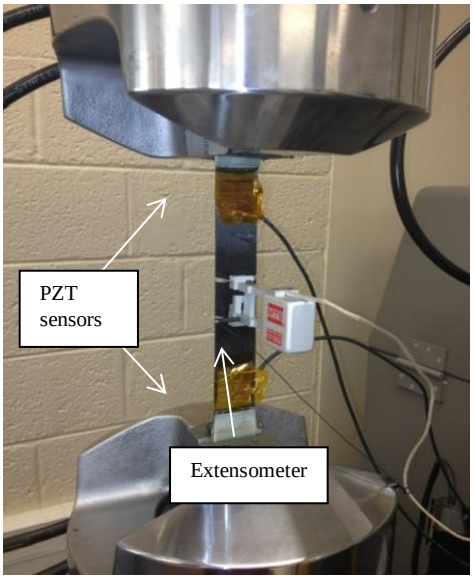

Figure 4.4. Tension specimen loaded in MTS machine

4.2.2 Fatigue Tests

To understand the response of composite materials to dynamic loading, several fatigue tests were conducted for both the cross-ply and quasi-isotropic specimens. The specimens were prepared in the same manner as the static test specimens in terms of tabbing and sensor attachment. Acquisition parameters and amplifier gain were also the same. The MTS-810 machine was used but with a cyclic tension-tension loading sequence. Various parameters of testing were controlled, such as the set-point load, load amplitude, and loading frequency.

For most cases, the set-point load was chosen so that the max amplitude was between 60-70% of the ultimate load. The maximum and minimum load were constrained by maintaining a stress ratio of 0.1 ($R=L_{max}/L_{min}$). A loading frequency of 5 Hz was used and the AE signals generated during testing were recorded.

4.3 Data Analysis

4.3.1 Static Tests

After preliminary tests were done to determine the strength of the cross-ply and quasi-isotropic, a total of ten (5 cross-ply, 5 quasi-isotropic) static tests were completed. Each test involved using two bonded sensors and two ultra-sonic sensors to record the AE events. The cross-ply specimens and the quasi-isotropic specimens failed at around the same load level, even with the cross-ply coupons being almost 25% thinner than the quasi-isotropic ones. This is attributed to the cross-ply coupons having more 0° degree plies which predominately carry the load. Table 4.2 shows the results from the static tests.

Table 4.2.

Failure loads of individual tension specimens

Tension tests					
Cross-Ply			Quasi-Static		
Test No	Specimen	Failure Load (kips)	Test No	Specimen	Failure Load (kips)
1	B2	9.13	6	D2	9.60
2	B3	9.80	7	D3	8.20
3	B4	10.00	8	D6	9.40
4	B5	9.75	9	D8	9.32
5	B7	10.00	10	F4	9.10
Average per 1” width		9.87	Average per 1” width		9.1

The data from the quasi-static tests were evaluated by plotting a combination of parameters: amplitude vs load, number of AE events vs load, etc.. For cross-ply and quasi-isotropic specimens, it was expected that various AE parameters, such as duration or frequency, would show obvious differences due to the failure process of each. Such as, yielding of the transverse matrix material, which theoretically should produce longer duration signals with moderate frequency content compared to fiber breaks, should occur more in quasi-isotropic

specimens due to the presence of the angled plies. This would lead to much more matrix crack signals in comparison to the cross-ply material. Quasi-isotropic specimens exhibit more delamination as well which should show distinct AE signals. Fiber break signals were not as obvious and required more assessment. Such signals will predominately occur in bulk right before failure since the fiber is the final constituent to carry load within the material. The amount of energy seen in a waveform generated from a certain failure mechanism is directly proportional to the energy release by that mechanism and the area of release. Thus, fiber breaks should generate relatively lower amplitude, very short duration, high frequency signals since the diameter of the carbon fibers are very small compared to the area of matrix crack growth. Figure 4.5 shows the difference between brittle fracture of a cross-ply specimen and delaminated failure of a quasi-isotropic specimen.

a) 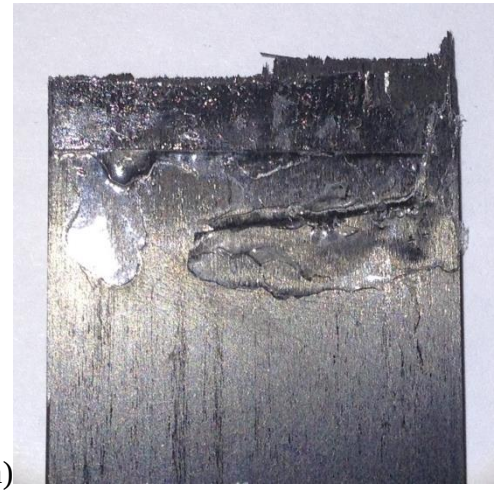 b) 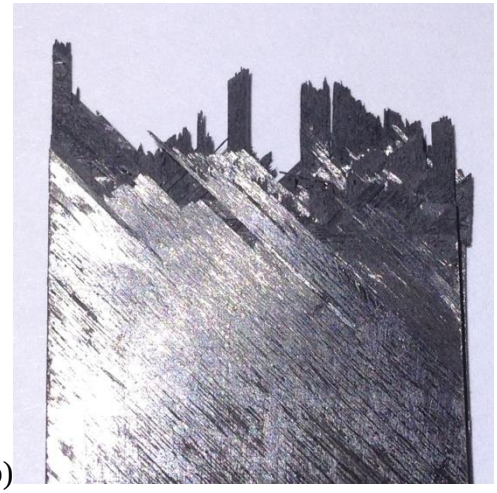

Figure 4.5. a) Brittle failure, b) Delaminated failure

The objective was to use the knowledge of where major failure mechanisms occur in terms of loading to isolate each. Such as, bulk matrix failure will occur around 20 – 40% of the failure load during static-loading while fiber breaks will dominate right before final failure. Noticeable delamination may occur around medium load level and grow up to final failure. An

inability to distinguish the AE signals can be attributed to a number of sources: insufficient acquisition parameters, frequency response limitation of the sensors, frequency damping due to attenuation, and signal attenuation/distortion due to damage.

The first step in accurately analyzing the AE signals is to deal with the impact of the acquisition parameters used on the different AE parameters. For example, a threshold must be set to trigger the system to measure an event. However, the threshold is mostly static and while it would suffice when measuring large amplitude signals, lower amplitude signals or signals that barely cross the threshold will yield parameter values that may not accurately describe the event, Figure 4.6. It is seen how sensitive some AE parameters are to the threshold. Duration and counts, which in some cases is used to calculate frequency, are important parameters in distinguishing features of various signals and should be calculated as accurately and meaningfully as possible. Normalizing the waveform then applying a relative threshold ensures that the features of the signal will be appreciated.

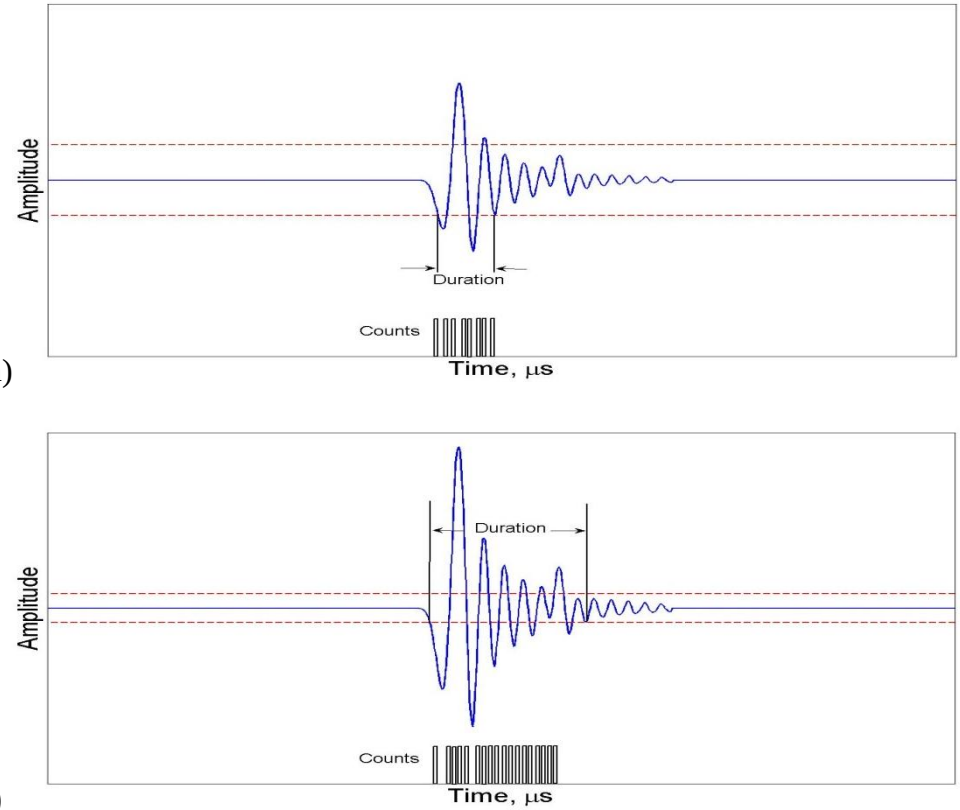

Figure 4.6. Effect of threshold on same waveform: a) original waveform, original threshold, b) normalized waveform, 10% threshold

As shown above, the threshold affects the measurement of the other AE parameters such as duration, energy, and count. A threshold that is too high results in the inability to measure relevant signals of low amplitude. If the threshold is too low, there is a risk that it may go below the noise ceiling and begin false signals which corrupt the measured data. This affect undoubtedly played a part in the inability to distinguish the failure modes using AE feature values. To make up for this, a MATLAB code was developed to reanalyze the raw data from each static test; the code can be seen in Appendix A. First, the raw waveforms corresponding to each AE hit/event were exported. The waveforms are then loaded in Matlab and individually analyzed through normalization. Normalizing the waveform gives the ability measure some of the various AE features such as duration, count, and average frequency but amplitude based

parameters become irrelevant, such as amplitude, energy, and RMS. A threshold is used to extract the AE features and it should be noted that the threshold was chosen so that the major peaks of the event will cross. These major peaks are typically between 10 – 20% of the maximum amplitude of the signal, therefore the threshold fell within that range. The next step involves directly measuring the parameters of the normalized signal.

In addition to finding the more realistic values of each AE parameter, a secondary procedure was done to account for occurrence of multiple events with a single measurement window. Ideally, a single event would occupy one measurement window but when AE signals occur in rapid succession, the result is multiple events within the window. The standard analysis software either ignores the latter events or considers them as one event. A "windowing" technique was developed and used to make use of the other events. Such a technique is necessary during the rapid damage growth that precedes final failure of composite materials. Figure 4.7 shows the result of using this windowing technique.

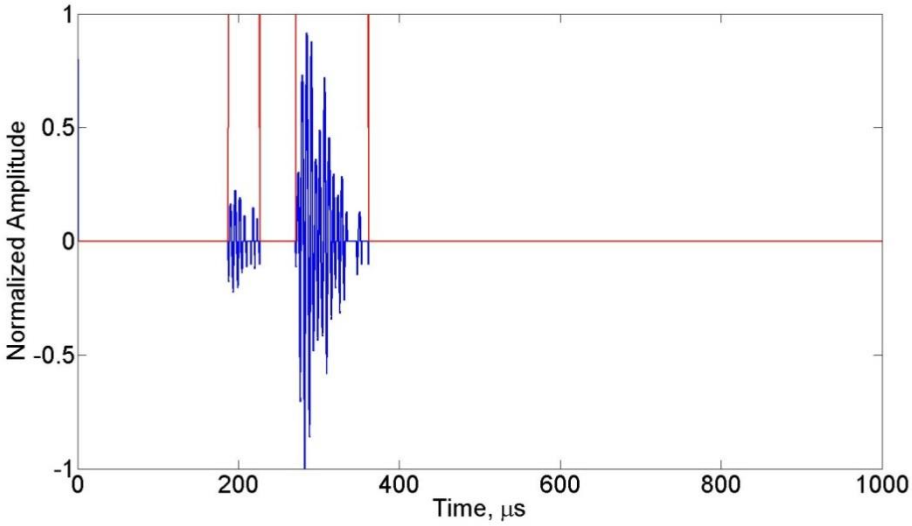

Figure 4.7. Windowing (in red) technique to extract AE events.

Having the ability to customize how the waveform data is analyzed gives a lot of flexibility and versatility. More so, when the material is close to failure, the events occur at a rate where it is

impossible to avoid capturing multiple events in a single window. This analysis can be adapted to any test data where more control is needed over how the information is extracted. The following sections show the results of the aforementioned algorithm that re-processes the waveform data.

Cross-ply: The failure of cross-ply composites is known to be dominated by fiber breakage. Therefore, while there will be significant matrix cracking at lower stresses, fiber break signals should be seen in bulk at higher stresses, particularly before failure. Several AE parameters of the cross-ply data were plotted and can be seen below, Figure 4.8 and 4.9.

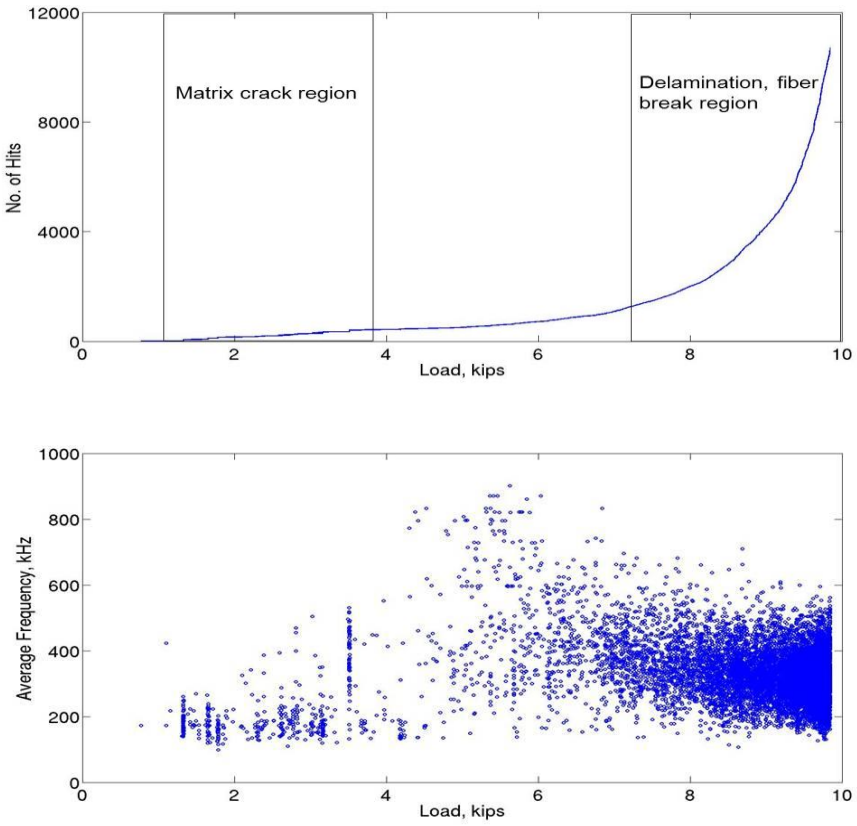

Figure 4.8. Number of hits and average frequency vs load

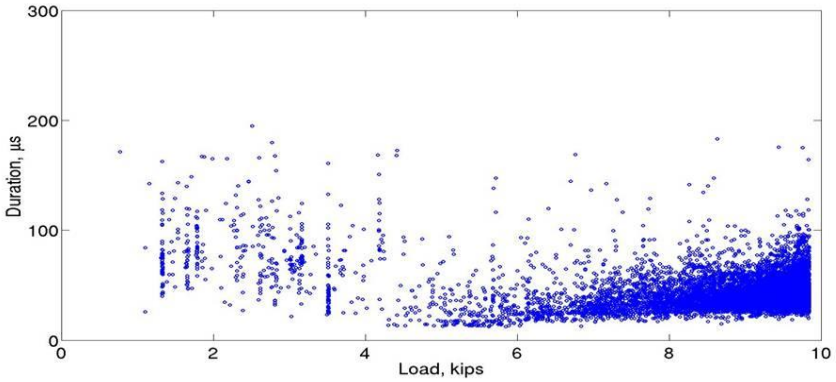

Figure 4.9. Duration vs Load

The results of the above plot show the resulting AE signals from the cross-ply specimen during quasi-static loading. First, a hit vs load plot depicts the separate regions where the different failure modes are likely to occur. Matrix failure will dominate the first region and generate a significant amount of transverse matrix crack signals which causes sudden increase in the number of cumulative signals. The second region, while there will be delamination, is dominated fiber breakage. Since damage is accelerated when fiber clusters fail, the number of events increases exponentially until failure. Between the two regions, there is an expected region of sustained damage growth where the number of AE signals linearly increases with the load.

Based on the physical phenomena of matrix failure and fiber breakage, the two should generate noticeably different AE signals in terms of frequency and duration. The second plot shows the average frequency vs load. The events within the matrix failure region tend to have an average frequency lower than the events within the fiber break and delamination region. The duration vs load plot show the events within the first region having an longer average duration than the later events. The characteristics seen in the above plots reinforce the concept that the physical phenomena of the different types of damage modes dictate the features that are seen in the AE events.

Quasi-isotropic: In contrast to what is seen during the failure of cross-ply composites, delamination is the most dominant failure mode for this layup. There will be more yielding seen in quasi-isotropic composites than in cross-ply composites. It is expected that there will be significantly more matrix cracking as a result. As with the cross-ply data, several AE parameters were plotted for the quasi-isotropic data, Figure 4.10.

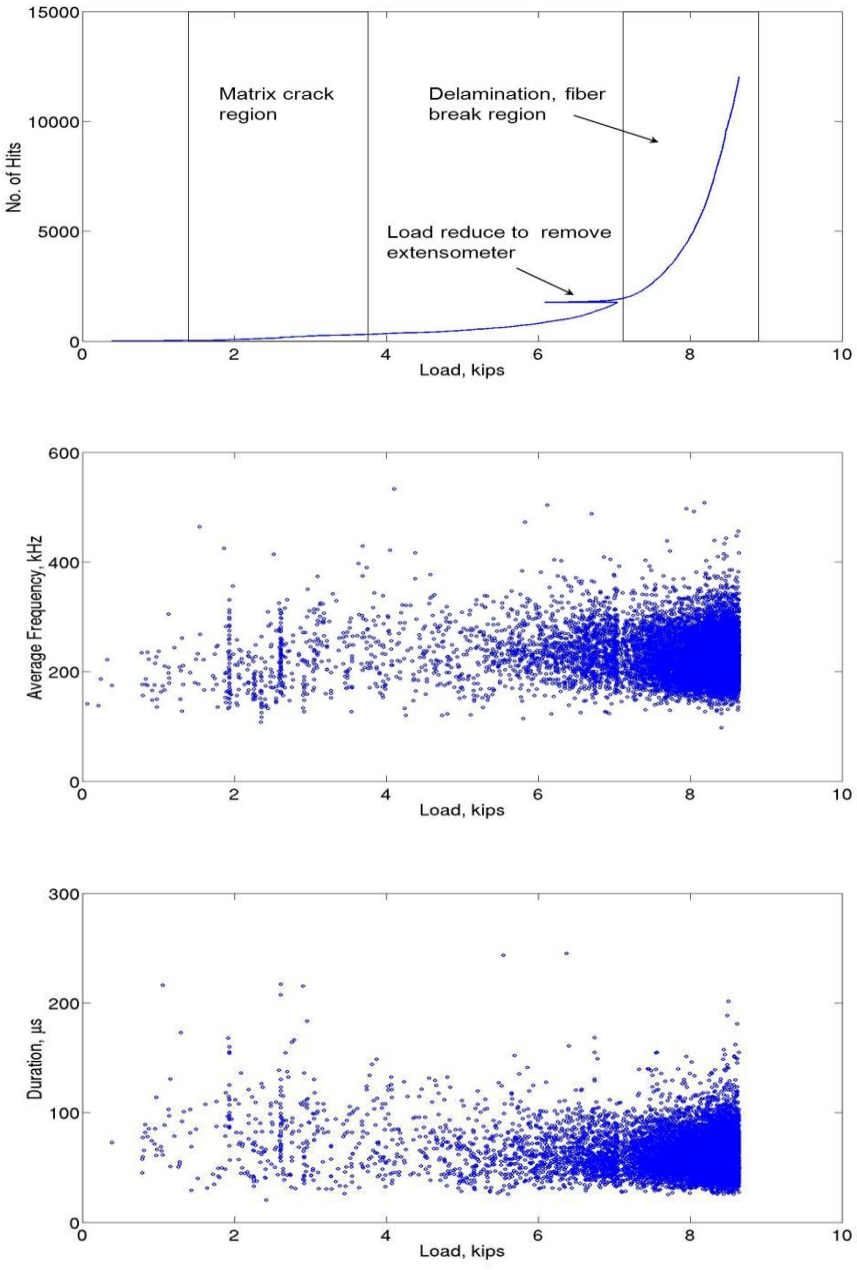

Figure 4.10. AE parameter plots for quasi-isotropic specimen

The number of events vs load for the quasi-isotropic resembles it's cross-ply counterpart in that there are two visible regions. In addition to transverse matrix cracking, there will be splitting of the 45°plies. Unlike the cross-ply plots, the average frequency/duration vs load plots do not clearly showcase the different features of lower and higher load events. This can be attributed to the dominance of delamination in the quasi-isotropic material. While simulated delamination signals show that the beginning portion of the signal does contain high frequencies, the second segment contains lower frequencies that will cause the average frequency to be similar to matrix crack signals. The duration range of matrix crack and delamination signals appear to be the same as well.

Cross-correlation of AE signals

The various AE parameters were expected to accent the different failure processes seen in cross-ply and quasi-isotropic. However, from the above plots, it is seen that these differences do not show up as clearly from an AE standpoint as previously thought. A detailed analysis including comparison of the different waveforms measured resulted in the same conclusion. Using just the AE features to identify the different failure modes was insufficient and did not provide enough distinction between each other.

A new approach was needed to extract useful information from the AE waveform data. To do so, the physical phenomena of damage growth in composites was revisited. It is known that after the initiation of damage, matrix cracks link up and lead to localized fiber-matrix debonding or, more importantly, delamination. Also, at high stresses, neighboring fibers begin to fail nearly simultaneously in localized regions. There will be multiple fiber failures known as multiplets, which are critical damage precursors to final catastrophic failure. Using this localized

nature of damage growth, a cross-correlation technique was developed and used to quantify this process.

A cross-correlation technique that measured the likeness or similarity between two data sets was used to analyze the AE waveform, Equations 1-2.

$$1)\quad R_{xy}(m) = E\{x_{n+m}{y_n}^*\} = E\{x_n{y_{n-m}}^*\}$$

$$2)\quad \hat{R}_{xy}(m) = \begin{cases} \sum_{n=0}^{N-m-1} x_{n+m}{y_n}^* & m \geq 0 \\ \hat{R}^*{}_{xy}(-m) & m < 0 \end{cases}$$

$$c(m)=\hat{R}_{xy}(m-N) \qquad m = 1,2,\dots 2N-1$$

where, *x* and *y* are two continuous functions representing waveform data, *E* is the expected value resulting from comparing *x* and *y*, *m* is the lag or shift, and *c* is the correlation array, each value of *c* corresponds to a certain lag *m*

Having the ability to account for the properties of wave propagation made this procedure ideal for AE data. For example, each failure mode should generate a unique signal with respect to the AE parameters. But two AE signals from the same failure mode will appear different for several reasons: the propagation path of each are different, dispersion, and attenuation. Therefore, signals that correlate at a high percentage must not only be of the same failure mode but also from the same localized region. This gives the ability to group or cluster the signals resulting from the different failure modes. Since the rate of damage growth increases as material gets close to final failure, monitoring the rate of cluster growth as well as cluster size gives the ability to determine when the composite is close to failure.

Correlation is usually done using some reference data to which the correlated data is compared. The reference data would have to account for the different aspects of AE data such as the source to sensor distance, depth, direction of growth and so on. Accounting for all these

aspects is impractical and very computationally inefficient. In order to have fast and efficient correlation, an “on-the-fly” correlation technique was developed. The following Figure 4.11 gives an example of how this technique works.

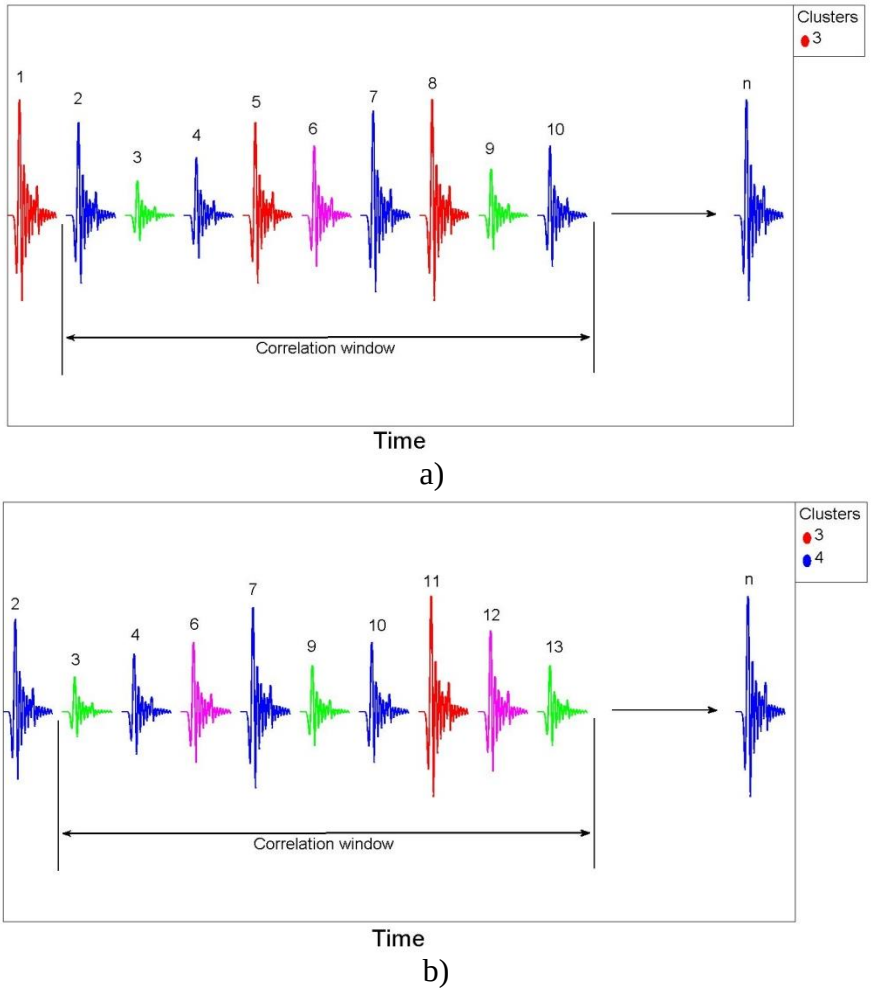

Figure 4.11. Illustration of correlation technique: a) 1st iteration, b) 2nd iteration

The above figure depicts how a group of arbitrary waveforms are correlated and clustered. Different colors represent waveforms gathered over a certain time frame. To begin, the first waveform was chosen as the reference waveform and a set number of subsequent waveforms are compared to it. If any of subsequent waveforms correlate at a predetermine value, the reference waveform and the matched waveforms are extracted and form a single cluster, shown as waveforms 1, 5, and 8 in Figure 4.11(a). After extraction of these waveforms, the

remaining waveforms slide in to occupy the void left by extracted waveforms. Now, waveform 2 in (b) is the reference and is correlated to subsequent waveforms for the second iteration of the code. Notice that the numbering of the subsequent waveforms will change as waveforms are matched and extracted. This process was repeated until the minimum number of waveforms needed for correlation was no longer met or until the specimen fails. Figure 4.12 and 4.13 also show not only the cluster but the size of the cluster which is important in terms of damage growth.

The clusters resulting from correlation at 90% are recorded in a table with each column containing a list of matched waveforms. As mentioned above, the size of clusters are very important since the rate of damage growth is related to the size of clusters that are forming. The following figures detail how certain sizes of clusters grow, for both cross-ply and quasi-isotropic specimens, as the specimen, approaches catastrophic failure. Cumulative clusters of a given size are plotted vs load up until the specimens fail.

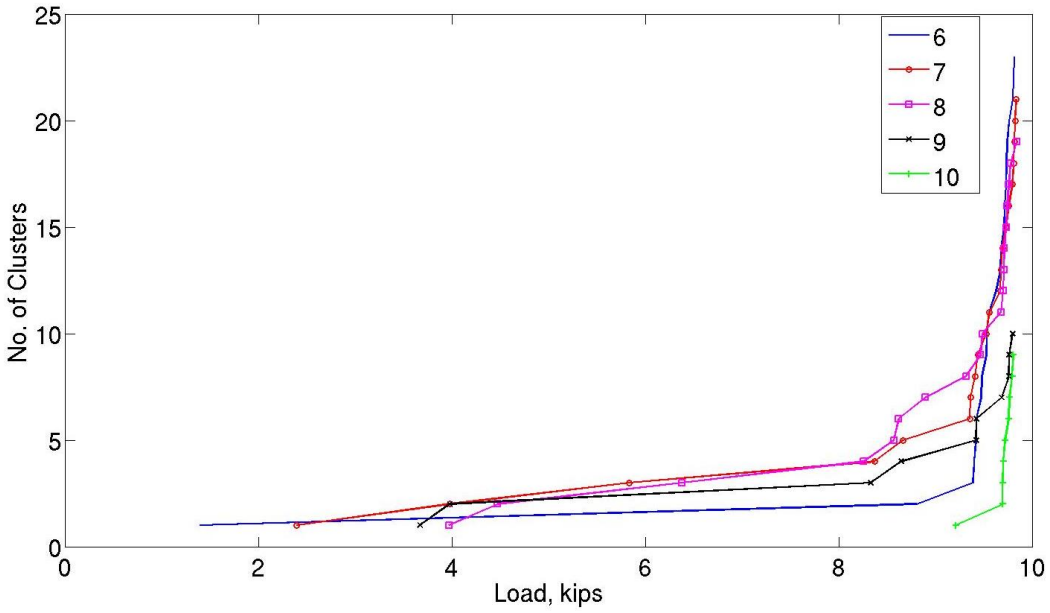

Figure 4.12. Cumulative cluster plot for channel 1

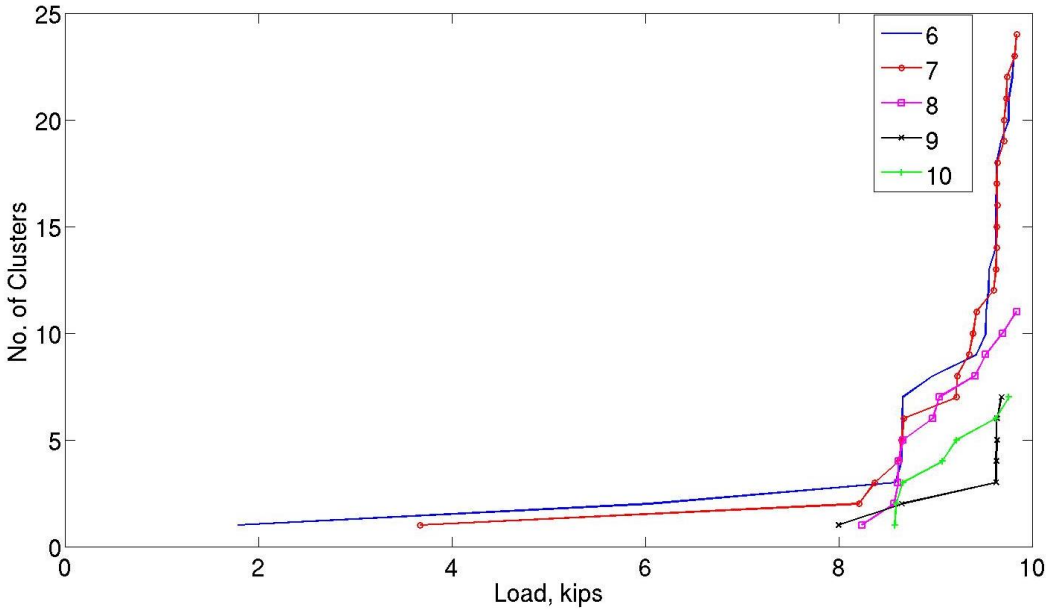

Figure 4.13. Cumulative cluster plot for channel 2

The cumulative plots for the cross-ply specimen show how the clusters of various sizes grow as the material gets close to failure. Comparing the trend of cluster growth to the trend in cumulative hits for these specimens, it can be seen that cluster growth is not sensitive to non-critical damage growth (matrix cracking) thus there is no initial stage of cluster growth at low loads. However, the clusters grew exponentially with the accelerated damage growth at high loads up to failure. Both channels for the cross-ply test showed clusters increasing around the same load. The next step was to find a relation between the characteristics of the clustered waveforms to the type of damage the material experienced. Figure 4.14 and 4.15 show common waveforms from early and late clusters, respectively.

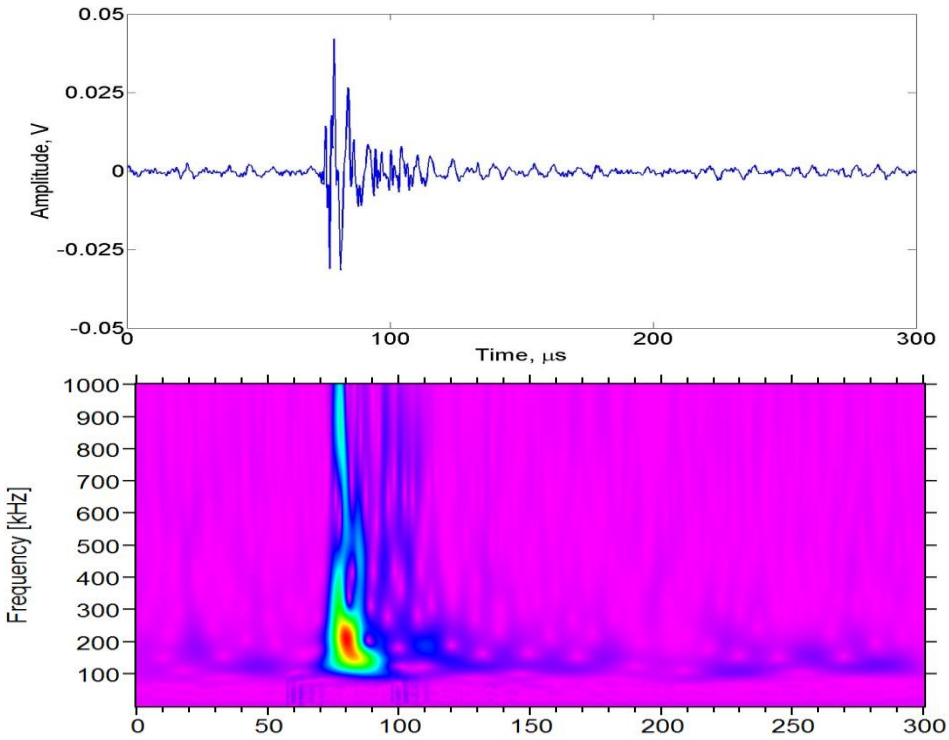

Figure 4.14. Typical waveform from early cluster and it's wavelet

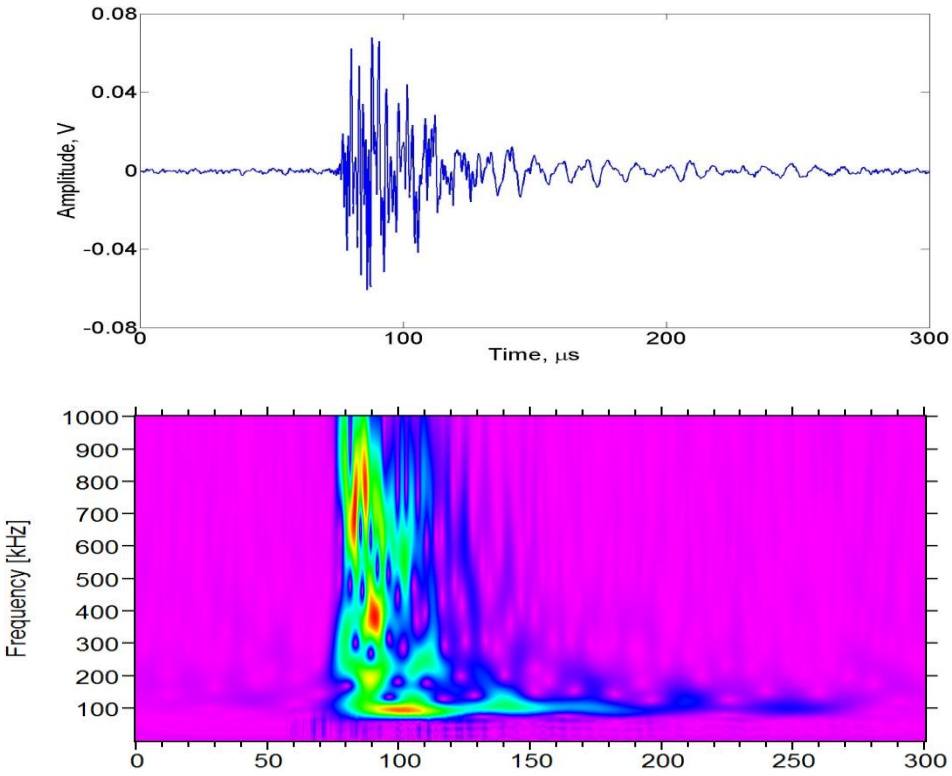

Figure 4.15. Typical waveform from late cluster and it's wavelet

The clustered waveforms seen in the cross-ply material show distinct features as the load increases. In early clusters, a high percentage of the waveforms have relatively short duration (40-50 μs) and contains a broad range of frequencies (100-800 kHz), as seen in Figure 4.14. Even though higher frequencies are seen in these waveforms, the lower frequency components dominate, which is typical of matrix cracking. However, with later clusters, the waveforms have a longer duration (75-100 μs) and have stronger higher frequency components. The occurrence of delamination and fiber breaks attributed to this phenomenon.

As seen in the figures for the cross-ply specimen, clusters for the quasi-isotropic specimen do not begin to grow until the stage of failure when critical damage growth dominates, Figure 4.16 and 4.17. Even though the same trend was seen for both layups, the cross-ply specimen data tends to show more of higher order clusters. A distinct difference in the quasi-isotropic data is the clusters waveforms seen at different load levels. Figure 4.18 and 4.19 show typical waveforms from an early and late cluster with their corresponding wavelets, respectively.

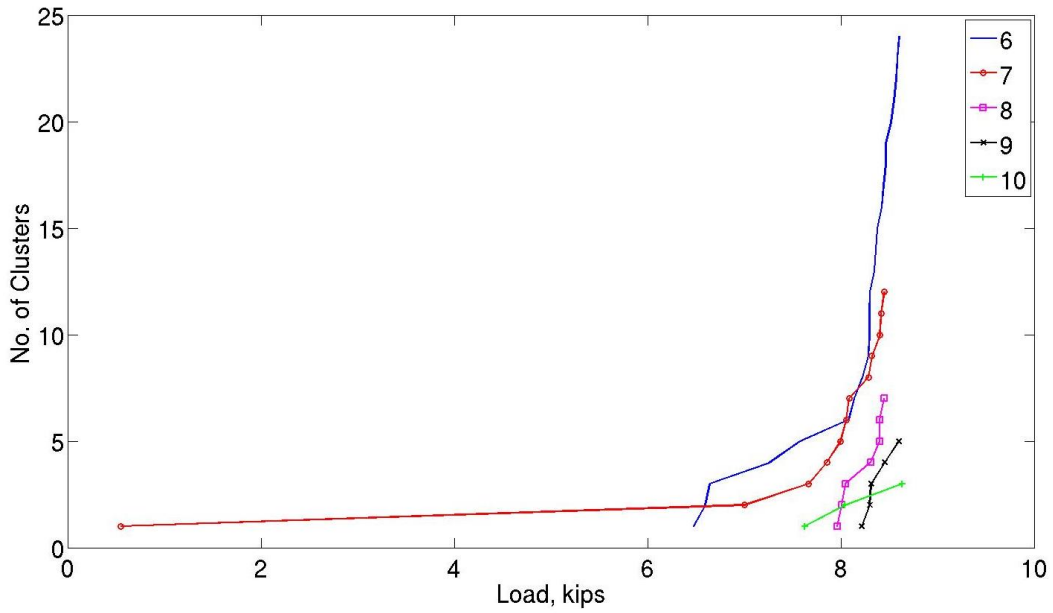

Figure 4.16. Cumulative cluster plot for channel 1

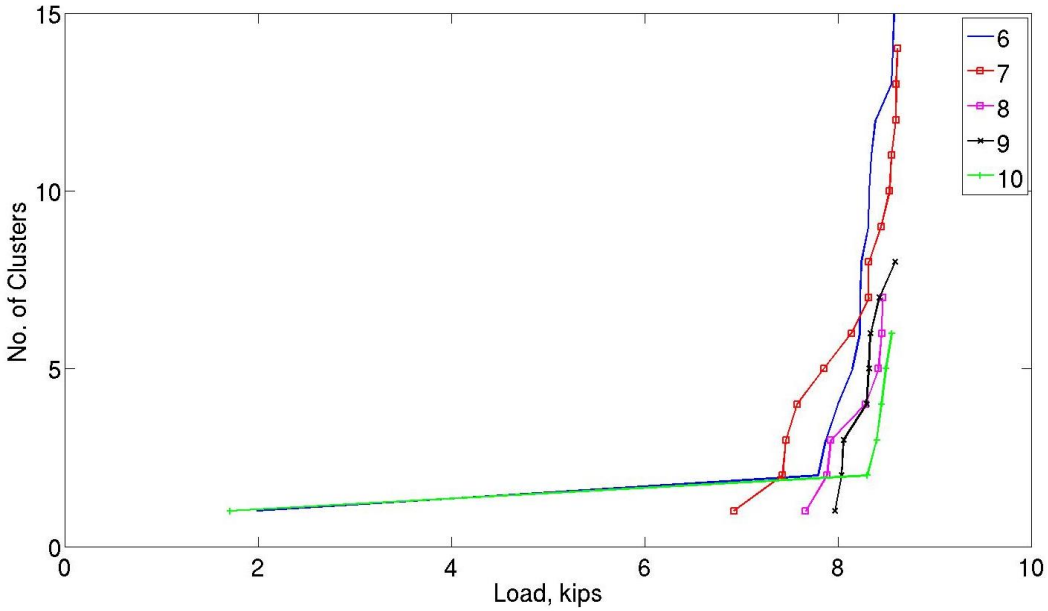

Figure 4.17. Cumulative cluster plot for channel 2

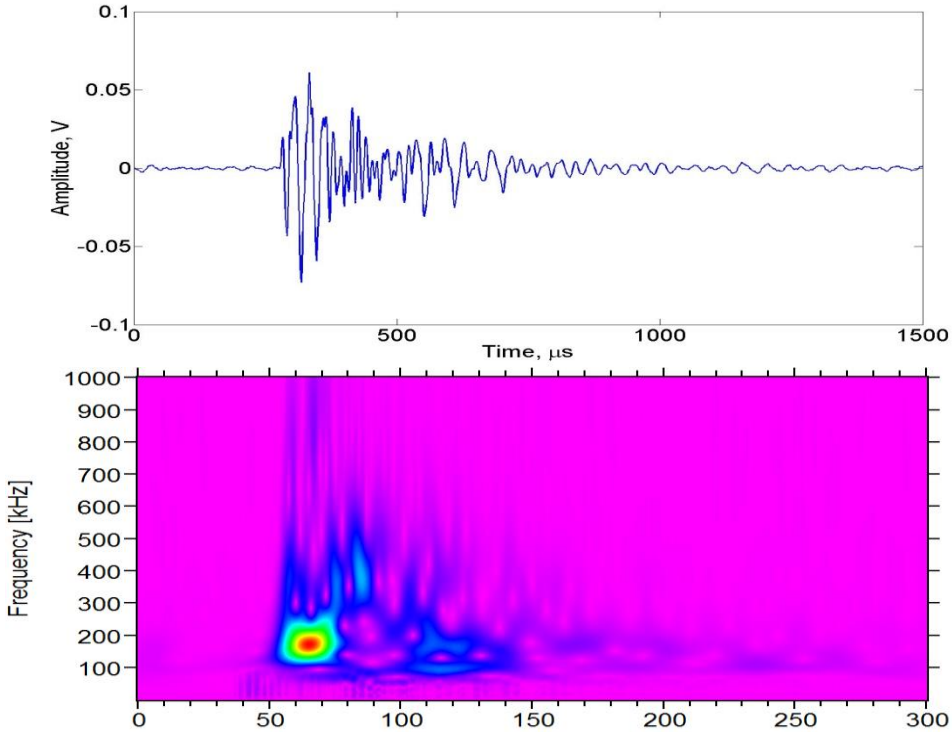

Figure 4.18. Typical waveform from early cluster and it's wavelet

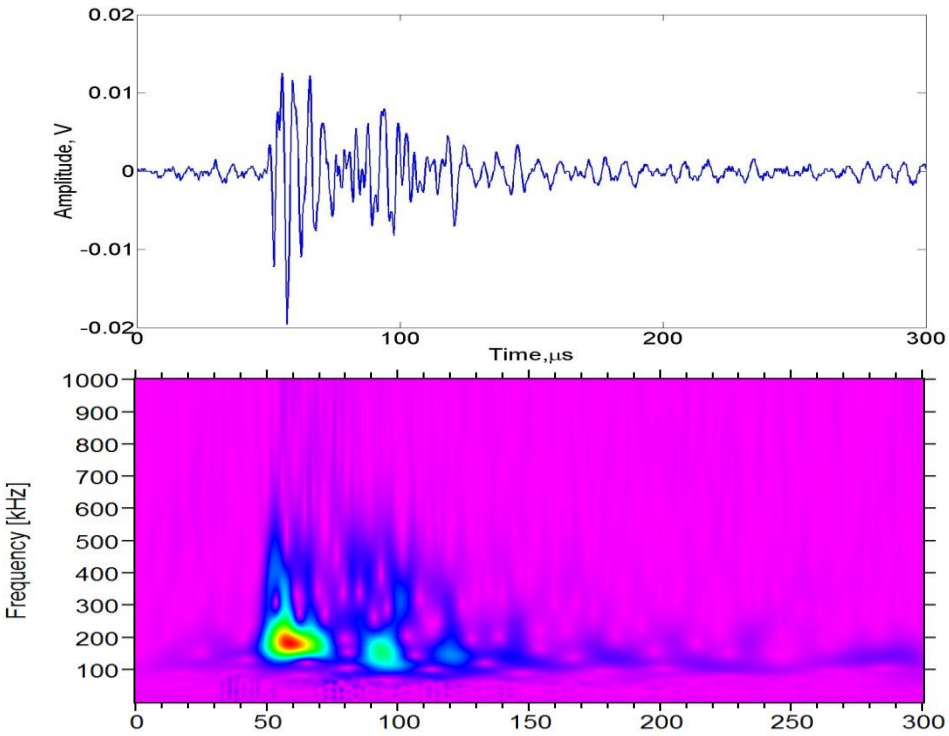

Figure 4.19. Typical waveform from late cluster and it's wavelet

The waveforms in early and late clusters do not show much difference in terms of their AE features, unlike the cross-ply data. Frequency content and duration of these waveforms stay in the range of 100-300 kHz and approximately 100 μs, respectively. Nearly all the clustered waveforms are dominated by low frequency components and have relative longer durations. Delamination is known to be the dominate failure mode in quasi-isotropic specimen and it was main source mechanism for the AE signals measured here.

4.3.2 Fatigue Tests

Damage growth seen during fatigue tests were much more exaggerated than during static tests. The main reason was that damage grows with each cycle and was allowed to propagate and coalesce since the applied stress does not exceed the strength of the material. Like the static tests, failure occurs in three stages but with fatigue test, damage growth and subsequent AE signals are continuous within the first and third regions. This creates data management issues for tests that

experience relatively higher number of cycles. Table 4.3 and 4.4 show the results of several fatigue test for both cross-ply and quasi-isotropic specimens, respectively.

Table 4.3.

Results for cross-ply fatigue specimens

Cross-ply Fatigue Data				
Specimen	**Load**	**R**	**Cycles to failure**	**Residual Strength**
B1	70%	0.14	26,067	
B6	50%	0.1	–	
B9	60%	0.1	–	116.5 ksi (-18%)
B12	70%	0.16	20,315	

The above table shows the test parameters for several cross-ply specimens. Two specimens failed at 20,000+ plus cycles when 70% cyclic load was applied. When 50% and 60% were used, the specimens were seen to have some damage initiated but not appreciable damage growth. Such loading conditions are thought to be within the endurance range and would only cause failure after an extremely high number of cycles. Specimen B9 was removed from cyclic loading and underwent static loading until failure. After undergoing a high number of cycles at 60% of ultimate stress, it failed under static loading at a stress of 116.5 ksi, an 18% reduction in the ultimate stress. The residual strength of the material was significantly affected even though the visible damage from fatigue loading was minimal. The AE data resulting from these tests was too large to be analyzed.

Table 4.4.

Results for quasi-isotropic fatigue specimens

Quasi-isotropic Fatigue Data			
Specimen	**Load**	**R**	**Cycles to failure**
F3	60%	0.19	271,348
F4	70%	0.2	17,960
F6	60%	0.18	112,000
F8	70%	0.16	12,055

All the quasi-isotropic specimens that were fatigue loaded failed. Only 60% and 70% cyclic loading were used since 50% did not produce failure within an acceptable time frame. The two specimens that were loaded at 70% failed before 20,000 cycles. Specimens F3 and F6 both were cycled at 60% and had similar stress ratio values of 0.19 and 0.18, respectively. However, specimen F3 failed after more than twice the number of cycles. The complexity of damage growth in composite makes it very difficult to predict the failure even when the loading conditions are the same. How damage evolves is very important in determining when a specimen will fail. As seen above, two specimens under almost identical loading conditions failed at vastly different cycles. The AE data from specimen F6 was the only fatigue data able to be analyzed, seen in the following figures. Figure 4.20 shows the number of AE events as the specimen was cycled.

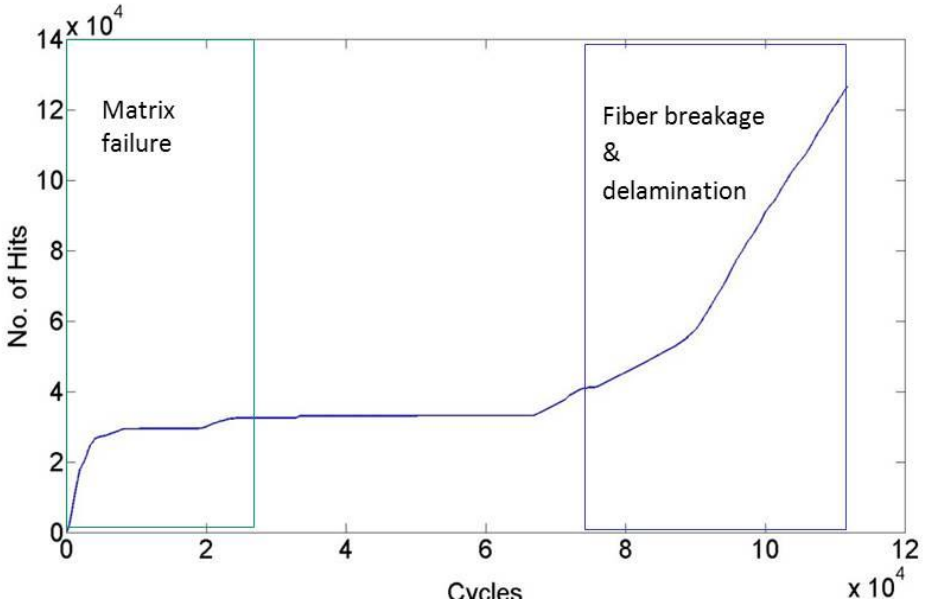

Figure 4.20. Hits vs No. of Cycles for quasi-isotropic fatigue specimen

Separate stages can be seen in the above plot, which is associated with the type of damage experienced in that region. The same three stage process seen in static testing was notice for fatigue testing. Again, the damage growth, particularly delamination, will be much more significant during cyclic loading. Matrix cracking will still dominate the first region and the middle stage is highlighted by minimal damage growth. Delamination and fiber breaks are seen in the later region.

Several AE parameters of the fatigue data were plotted below, Figure 4.21. There are two main groups seen in both plots, which correspond to the first and last stage of damage growth. No significant damage growth is expected in the middle region and therefore there are minimal AE signals.

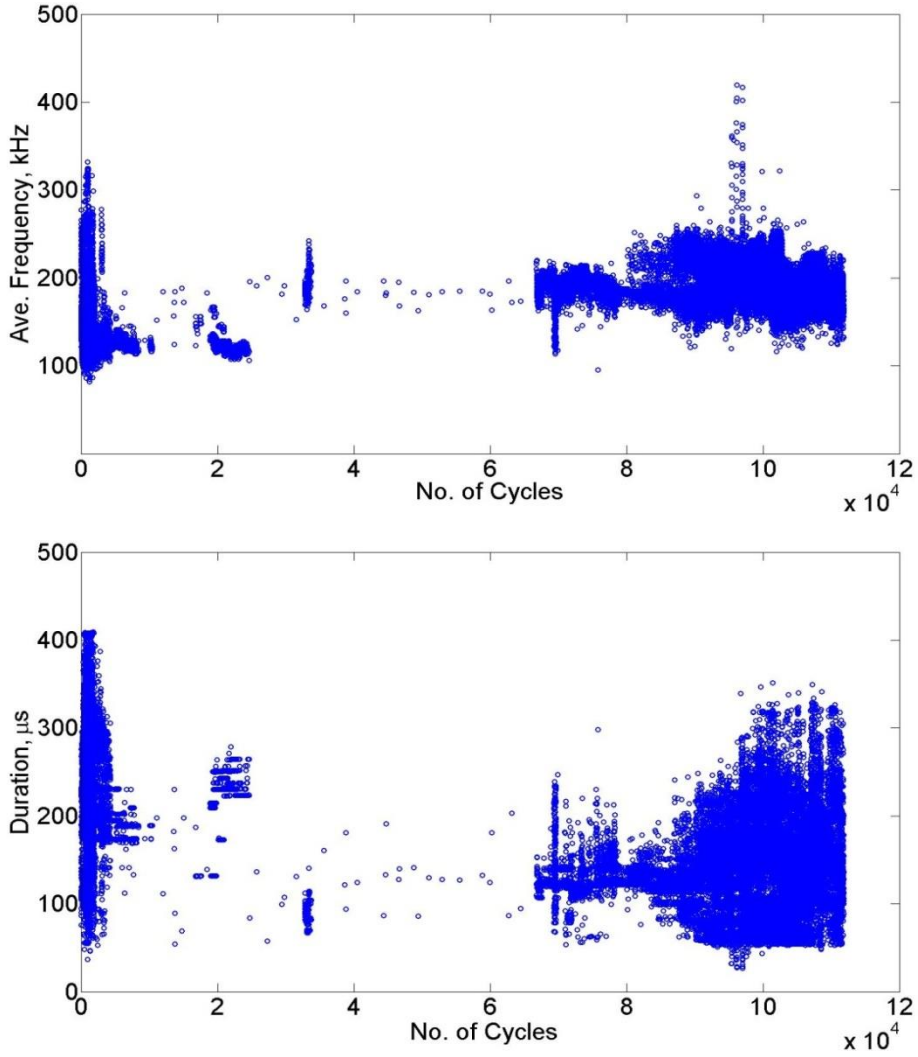

Figure 4.21. Average frequency and duration plot for quasi-isotropic fatigue specimen

Considering just the initial group and the last, the centroid frequency of the latter group is slighter higher than the former. The frequency band also is narrower for the end group. This was expected since the domination of delamination as well as the presence of fiber breaks will contain higher frequency components. The duration plot also showed characteristics expected during the failure of a quasi-isotropic specimen. A slightly lower centroid for the end group can be noticed but nothing appreciable. Like the AE parameter plots for the static specimens, there is not much information about critical damage growth gained from the above plots. Therefore, the

same correlation technique used on the static data was applied to the fatigue data. A correlation coefficient of 90% was used to cluster the data and the results can be seen below in Figure 4.22.

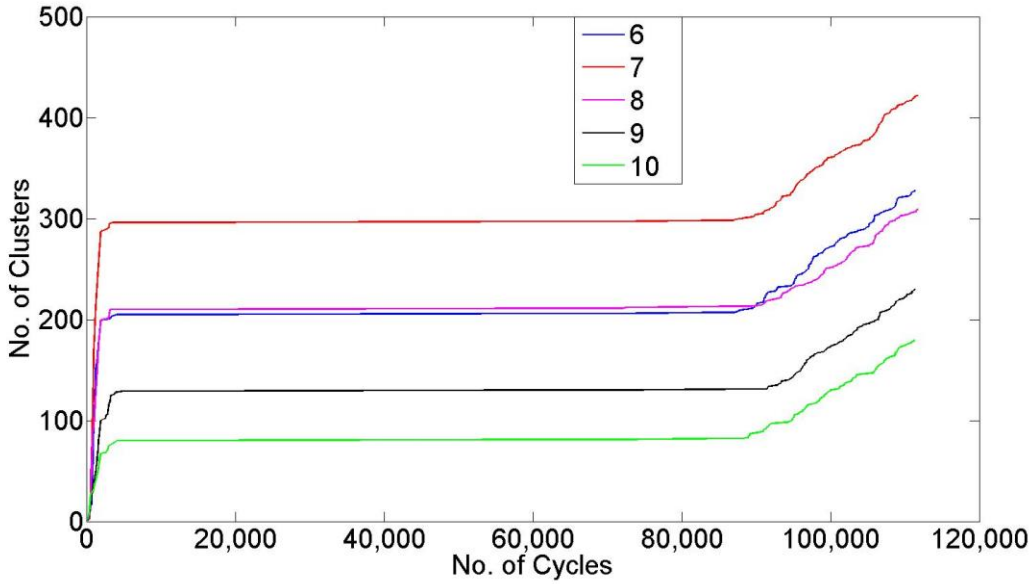

a)

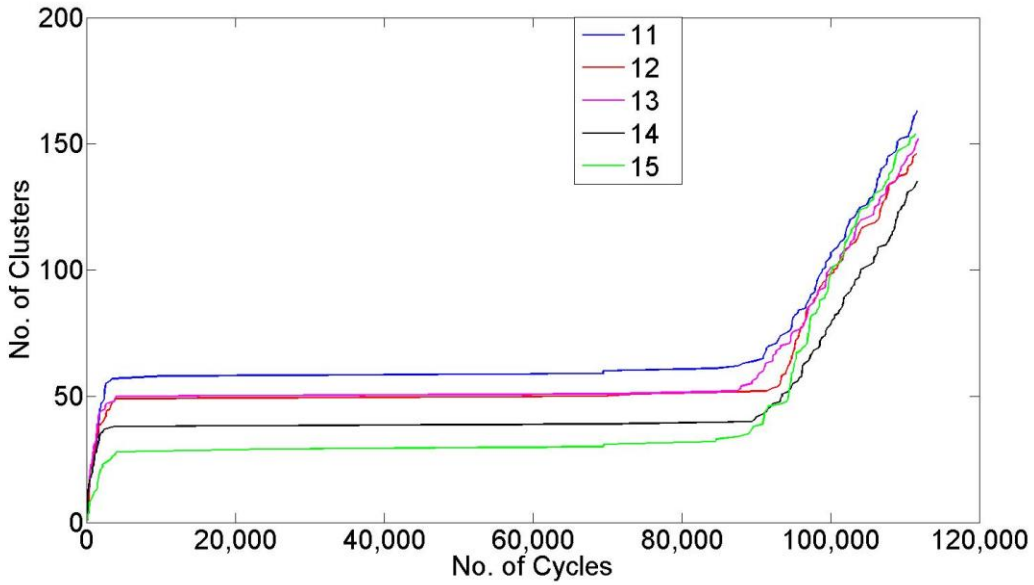

b)

Figure 4.22. Cummulative cluster plots for quasi-isotropic fatigue specimen: a) lower-order clusters, b) higher-order clusters

A key difference seen in the cluster plot for the fatigue data was the presence of the earlier clusters within the first damage growth region. Matrix cracking dominates this region and

did not produce any clusters from the static data. Ideally, clusters will only form in the final region of damage growth where critical damage occurs but there are a significant number of lower and higher order clusters in the first region. To understand why clusters form in this region for fatigue loading and not static loading, the nature of damage growth during static and cyclic loading must be revisited.

During static loading, a continuous load was applied until the specimen failed. Matrix cracking happens around the 20-40% range in random fashion in terms of location for the material tested. There will be linking up of these matrix cracks and saturation as the load increases and the occurrence of such signals will decrease dramatically afterwards. The fact that matrix cracking occurs so randomly means there will not be good correlation between the successive signals measured. However, when the static specimen gets close to failure, fibers begin to break. Neighboring fibers will fail in multiples and may give rise to delamination. Due to matrix crack saturation and the development of fiber breaks and delamination growth in a localized area, a high percentage of the successive signals measured will be from the fiber break/delamination region and will therefore correlate much better. This is why clusters only formed at very high load or close to failure for the static specimens.

The case was different for fatigue testing. There will be random matrix cracking in the early cycles because fatigue loading is typically applied at 60% or higher of the ultimate strength. Such loading exceeds the strength of the matrix and cracking will begin within the first cycle. While the matrix cracking that occurs during the first few cycles may be randomly distributed, there will be direct growth of these cracks due to cyclic loading. The direct growth and eventual linking up of these cracks will give rise to localized damage and will produce signals that correlate well, which can be seen in the above figures. There are clusters in the

beginning of cyclic loading due to matrix cracking but they cease after 5% due to saturation. After saturation, there was no cluster growth until around 80% of the failure cycles. This is where critical damage growth will dominate and in the case of quasi-isotropic specimens, severe delamination will be seen. Clusters can be seen growing all the way up to final failure and occur in very large number for fatigue loading. Only clusters sizes up to 15 are plotted but even larger numbers were noticed.

4.4 Summary

A series of quasi-static tension and fatigue tests were done for cross-ply and quasi-isotropic specimens. The dimensions of the specimens were determined using ASTM standards. The AE signals were measured using PZT bonded wafer sensors and analyzed using commercial AE signal analysis software. It was assumed that the different failure modes generate unique signals and can be quantified based on these features. Certain plots such as load vs or load vs amplitude give a slight indication of the features of matrix cracking and fiber break signals. However, the features do not show up as distinct as previously thought due to several aspects of wave propagation in composite materials, primarily during failure. Attenuation, wave scattering, and dispersion affect the measured waveforms and make it very difficult to determine it's original AE feature content. Having the ability to distinguish the signals of different failure modes depends on being able to measure that original content. Since this capability does not exist, the pattern classification became impractical. A new technique was developed to track the growth of critical damage.

The correlation technique used made use of the localized nature of damage growth. This technique was applied to the two channel data measured in cross-ply and quasi-isotropic. Both channels for each layup showcased the same trend of cluster growth within the region where

critical damage growth was expected. Having a technique that was sensitive to damage was very advantageous because while detecting damage was never a problem using acoustic emission, distinguishing between critical and non-critical signals was. The main difference between the data for the two layups was the cluster waveforms for cross-ply show different AE feature content at different load levels whereas the cluster waveforms for quasi-isotropic showed somewhat consistent AE features at all load levels, which could be due to the severe delamination seen in such material. Intermediate cluster sizes from 6 to 10 were plotted but larger cluster sizes were noticed. Larger clusters (11+) were also present but smaller in number. Critical damage growth in static specimens was captured using this clustering technique.

Like the static data, the AE features from fatigue test did not provide reliable information in terms of critical damage growth. The clustering technique used for static test data was applied to the fatigue data. While the technique was able to capture the critical damage growth before failure, there were clusters seen early in the loading process within the non-critical damage growth region. The cyclic loading caused the non-critical damage to propagate locally and ultimately generated cluster signals.

CHAPTER 5

AE in CFRP Panels

5.1 Introduction

This chapter focuses on measuring damage growth in CFRP panel that was loaded in the same quasi-static manner as the coupon tests. A quasi-isotropic panel was used with a $[+45/90/-45/0]_{2S}$ layup. A circular hole was drilled in the center of the panel to initiate damage growth and the corresponding AE signals were measured as it was loaded. The objective of this portion of the research was to monitor damage growth in a realistic aerospace component, which the panel represents. The clustering technique used for the specimen data was applied to the AE signals generated during the failure of the panel. Whether critical damage signals in large structures cluster together as seen in coupon tests was investigated in this chapter.

5.2 Test Panel and Procedure

The panel used was of the same makeup as the quasi-isotropic coupon specimens used for static testing. Dimensions of the panel were chosen such that it was large enough to represent a real aerospace component but small enough to be load to failure in the MTS machine. Figure 5.1 shows the dimension of the panel used. Tapered aluminum tabs were bonded to the panel using high strength epoxy to prevent stress concentration and possibly failure at the grips. Damage was expected to initiate and grow from the lateral sides of the circular hole and PZT sensors are placed at strategic locations to measure the AE signals in this area.

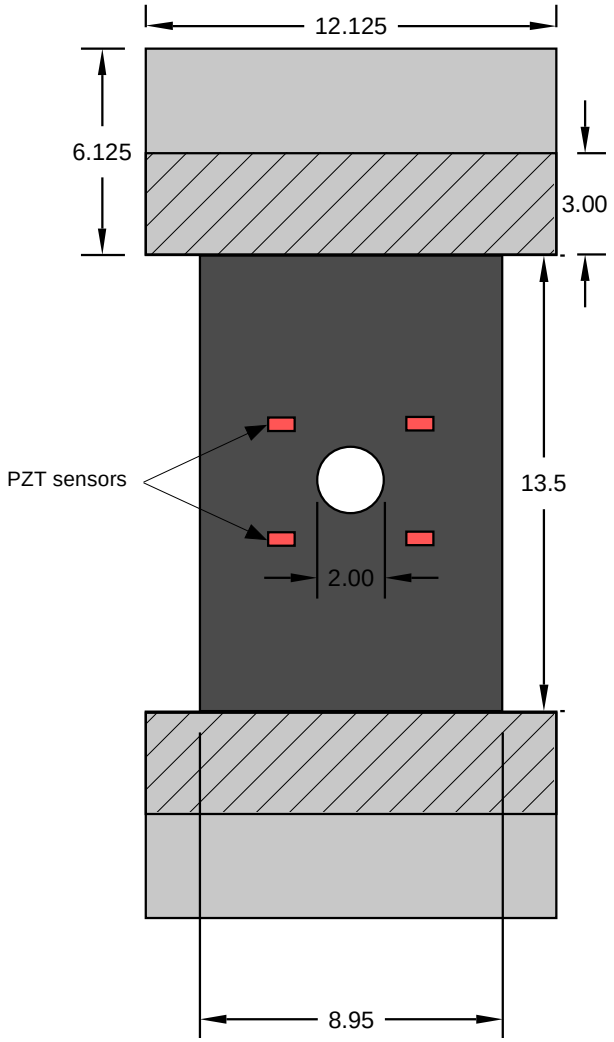

Figure 5.1. Dimensions of quasi-isotropic panel

As seen in the schematic above, four PZT sensors were bonded to the panel. Four sensors were placed at strategic locations around the circular hole. The top two were located 1.5 in above the transverse mid-plane while the bottom two were 1.5 in below this plane. Since damage was expected initiate and grow at the lateral edges of the circle, the sensors were placed at the optimal position to measure AE signals generated during damage growth. The sensors were located close enough to the damage area so that the effect of attenuation and reflections are minimal while being far enough to allow the Lamb waves develop.

Fiber optic sensors were also attached to the panel to measure the strain distribution around the damage area. Bragg gratings are contained in the fiber at 0.5 in increments for a total number of 140 gratings. The pattern used to attach the fiber was such that the uniaxial strain from around the circular hole to the edge of the panel would be captured using discrete points. Figure 5.2 shows a schematic of the fiber path. The green area shows the region of interest along the fiber for strain measurement.

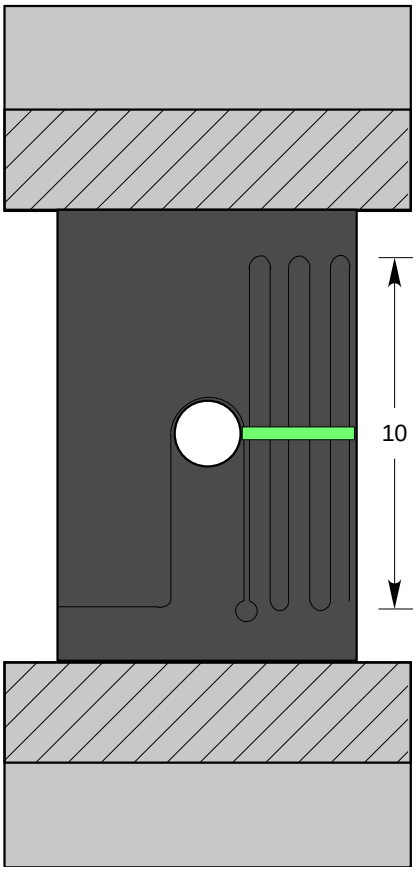

Figure 5.2. Fiber layout on panel

The panel was statically tested under load-control using the same loading rate as the latter tensile specimens, which was around 10,000 lbs/hr. This was done to allow a fair comparison to the earlier tests and to ensure consistency in damage growth. An unnotched failure load of 58,000 lbs was calculated but due to the stress concentration at the hole, the panel was predicted

to fail between 30-35,000 lbs. The acoustic emission signals were recorded by a PCI-2 data acquisition system. Each channel used a pre-amplifier at 40 dB gain and recorded signals up to 1 ms. A sampling rate of 5 MHz was used while having a threshold of 45 dB to ensure a good signal to noise ratio.

The fiber optic system was capable of a strain measurement rate of 30 Hz. Figure 5.3 shows the experimental setup used during this test. For the AE data, the PZT sensors measured the acoustic emissions as voltage vs time waveforms. The waveforms were then amplified at 40 dB using a PAC pre-amplifier and the amplified signals were recorded using the PIC-2 data acquisition system. A RTS150 fiber optic system was used to interrogate the Bragg gratings for strain measurement. A laser within the system sends out light over a predetermined wavelength range into the attached fiber and measures the reflected light. Strain data was recorded in 500 lb increments using LabVIEW. Strain data from these locations is plotted in the next section.

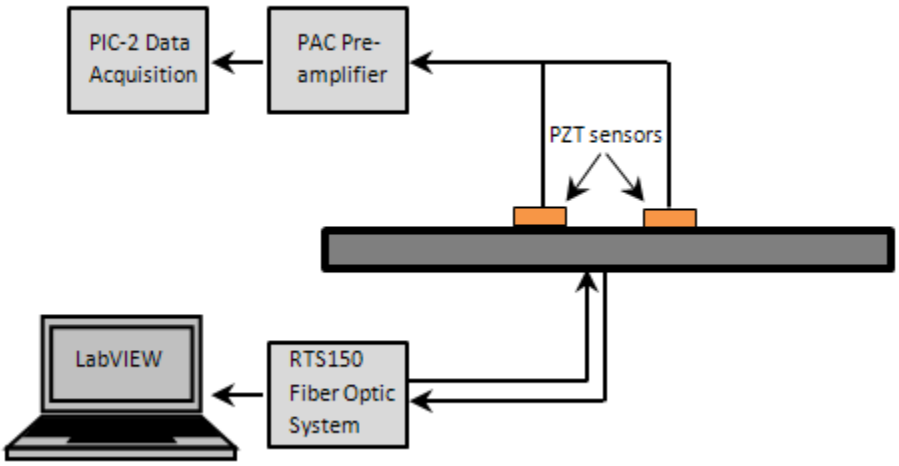

Figure 5.3. Schematic of experimental setup for panel test

5.3 Data Analysis

5.3.1 AE signals

The acoustic emission data was recorded for each channel during the entire loading sequence. Compared to the earlier specimen tests, the total number of hits was lower than expected but enough to capture the failure of the panel. Channel 1 and 2 recorded around 75% of the total events and thus displayed better results when the data was plotted. The panel failed in the middle through the circular hole as desired, Figure 5.4. AE waveforms were correlated in the same manner as the specimen test and clusters were generated. Figures 5.5 shows the total number of events measured by each channel while Figure 5.6 and Figure 5.7 show the clusters data for channel 1 and channel 2, respectively.

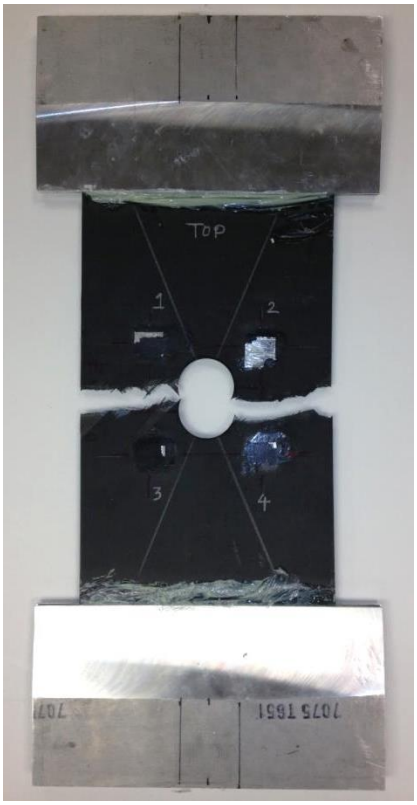

Figure 5.4. Quasi-isotropic panel after failure

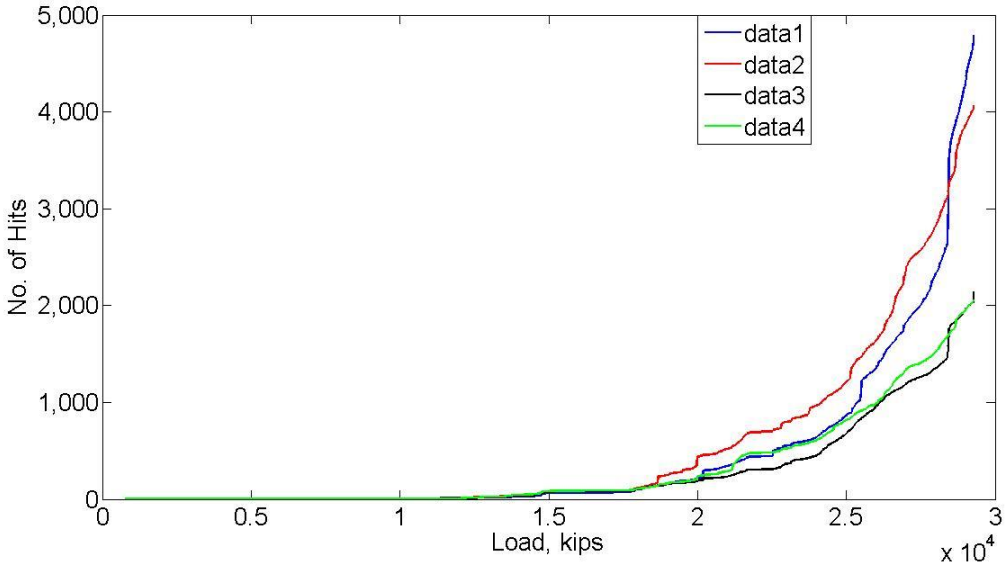

Figure 5.5. Hits vs Load for each channel

The trend of the number of hits for each channel was very similar which means all sensors performed consistently and reliably. It was also seen that the frequency response of each remained relatively intact. Figure 5.8 and 5.9 show the cluster data from channel 3 and 4.

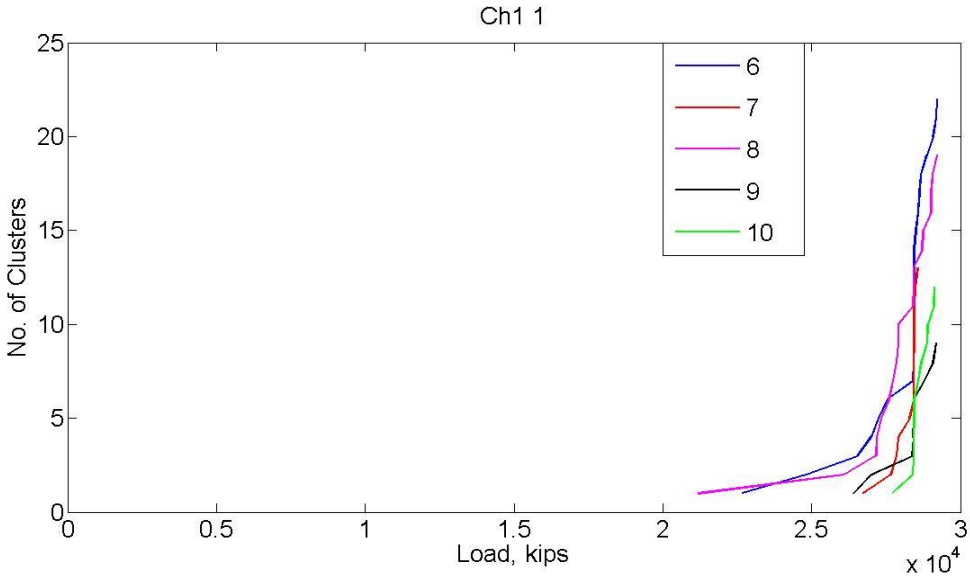

Figure 5.6. Cluster plot for channel 1

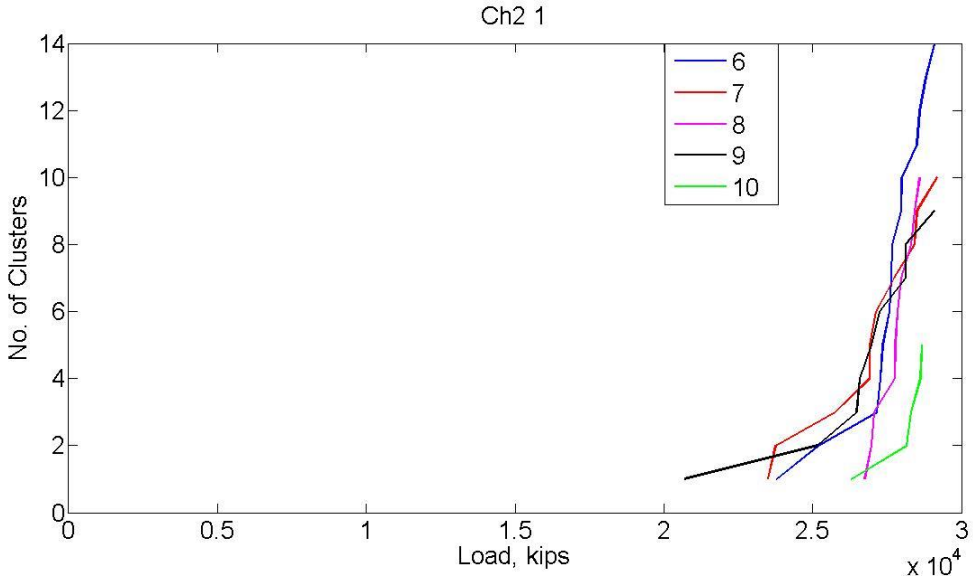

Figure 5.7. Cluster plot for channel 2

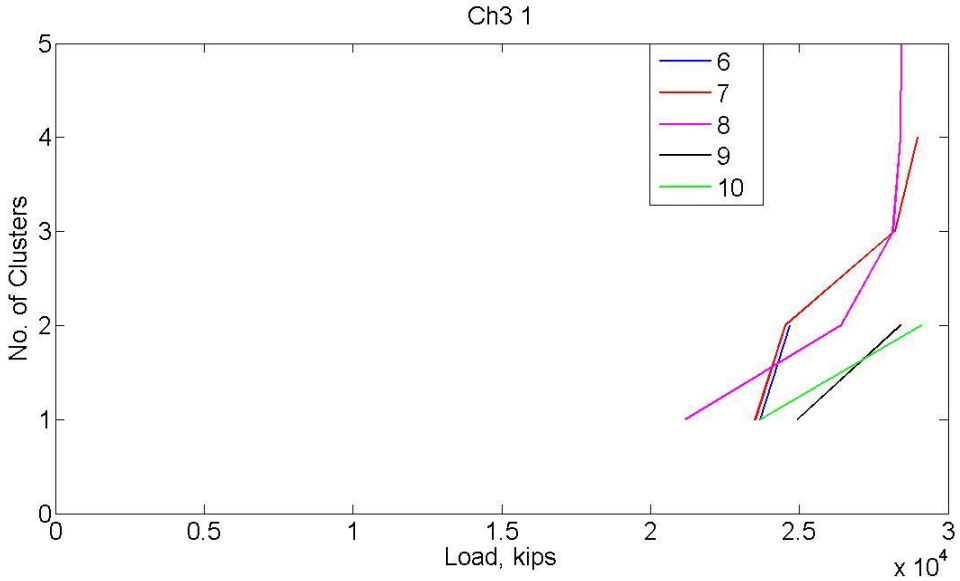

Figure 5.8. Cluster plot for channel 3

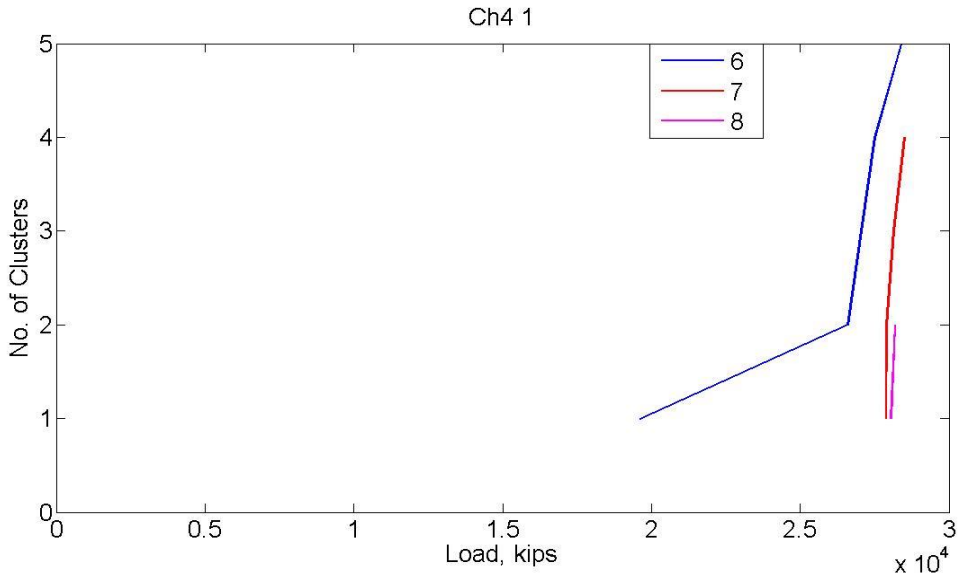

Figure 5.9. Cluster plot for channel 4

The above cluster data showed the same trend that was noticed in the specimen tests. Clusters formed in the later stage of loading close to failure and increase dramatically up to failure. Larger clusters (10+) were also seen but due to the low number of total event resulting from this test, those higher order clusters are low in number. Also, the clusters were found using a correlation of 90%. The sensitivity of channel 3 and 4 appeared to be low which lead to the low number of total hits for each channel and fewer clusters compared to channel 1 and 2. Figure 5.8 and 5.9 shows typically waveforms seen in early and late clusters, respectively.

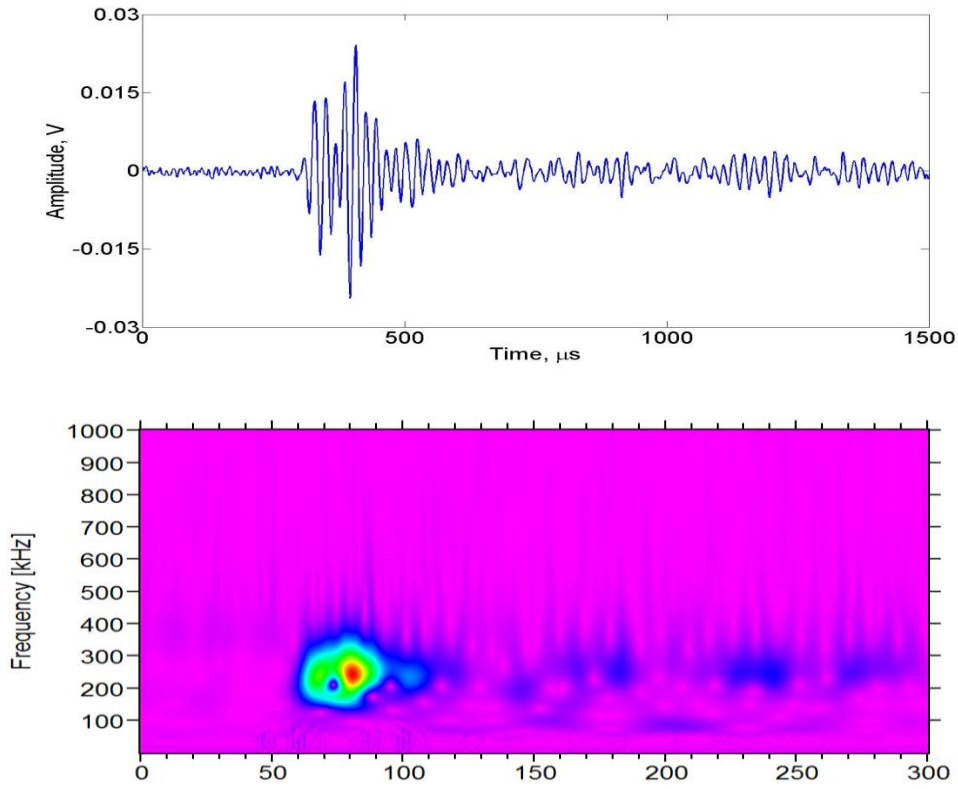

Figure 5.10. Typical waveform from early cluster and it's wavelet

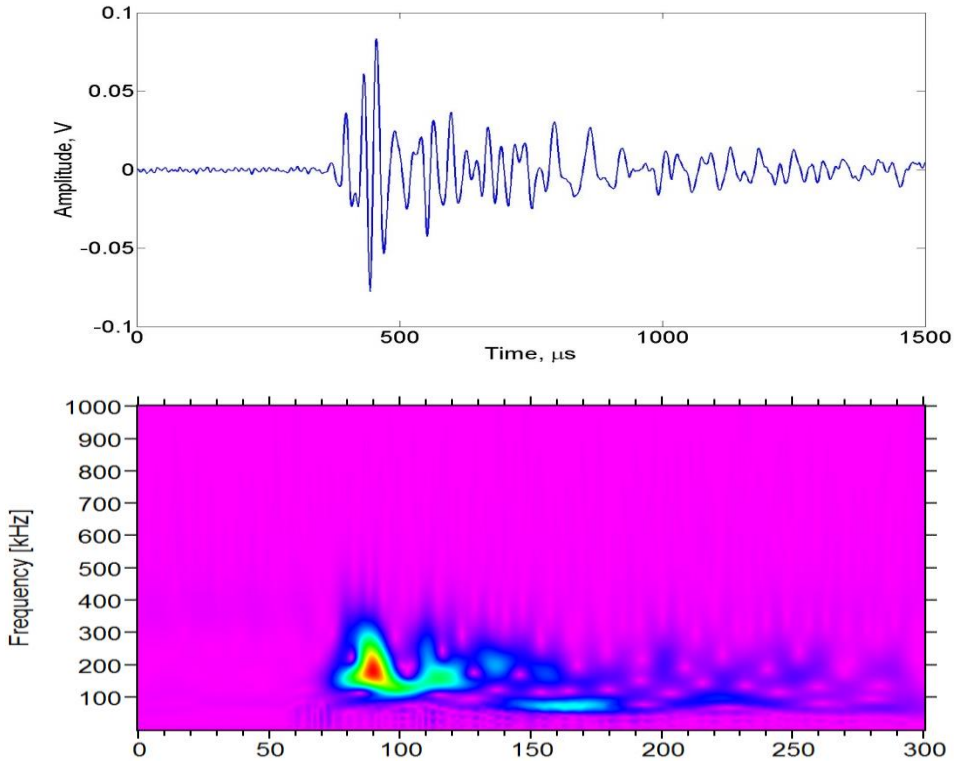

Figure 5.11. Typical waveform from later cluster and it's wavelet

The above figures show the frequency content of the cluster signals measured at low and high loads. As seen in the static tests for quasi-isotropic specimens, the frequency content remained within the same range of 100-400 kHz. The duration of the signals also remained around 100 μs. Again, this was attributed to the domination of delamination within these specimens.

5.3.2 Fiber Optic Data

As mentioned earlier, the fiber optic data was recorded up to 29,000 lbs in 500 lbs increments. The main objective was to measure the strain distribution as the panel was loaded and experienced damage. Strain measurements were taken at the discrete locations mentioned above. Stress concentration at the lateral edges of the circular hole led to high strain around this area. The raw strain distribution measured by the fiber optic sensors can be seen in Figure 5.10. The grating number was the successive sensor number along the fiber. When the strain wastaken from the desired locations, shown by the red dots, Figure 5.11 was obtained. The strain at those chosen location was plotted for different load levels.

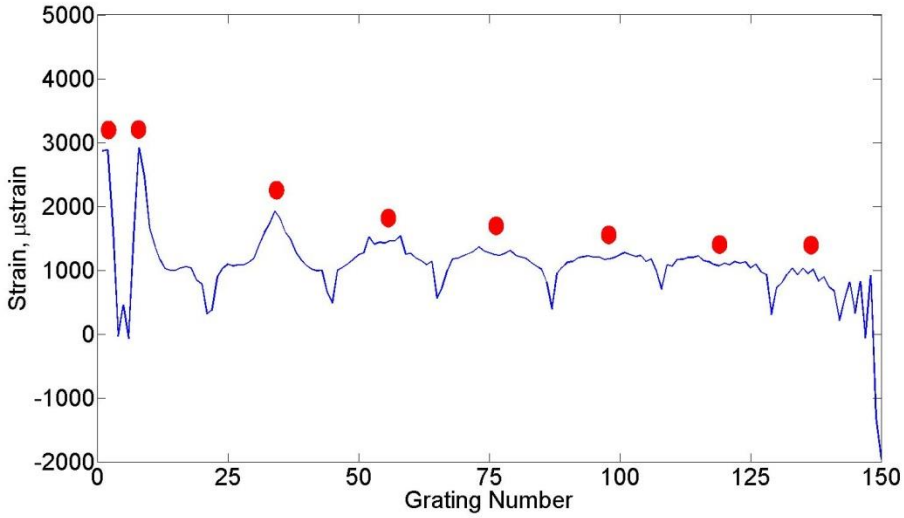

Figure 5.12. Raw data output from fiber optic system

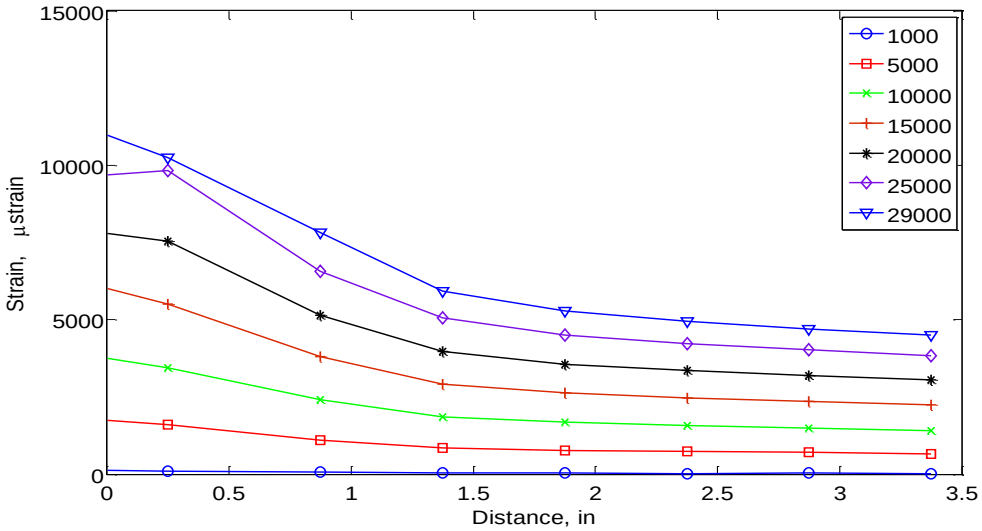

Figure 5.13. Strain distribution from circular hole to plate edge

The strain was plotted for the seven locations starting at the edge of the center hole. Distance from the lateral edge of the circle is shown on the x-axis with the first point being very close the edge of the circle, represented as zero. The near-field strain gradient at the hole was seen to be more than twice the far-field measurements close to the edge of the panel. At lower loads, this difference was not as noticeable. This was attributed to the localized stress concentration which only affects strain measurement within close vicinity of this area. The far field strain seen close to failure was almost half of what was measure at the edge of the circle. Failure of the panel occurred between 29,000 and 30,000 but the strain at failure was unable to be recoded due to sudden failure. Figure 5.12 shows the strain concentration at the circular hole. The values are obtained by dividing the strain measured at the edge of the circle by the strain taken at the edge of the panel. Initially, the strain concentration was above 3.5 but decreased and fluctuated until around 5000 lbs. This was due to the initial damage, which caused a redistribution of the strain concentration. As the load was increased, the strain concentration stabilized between 2 and 2.5. Therefore, the damage zone did not grow much before catastrophic failure.

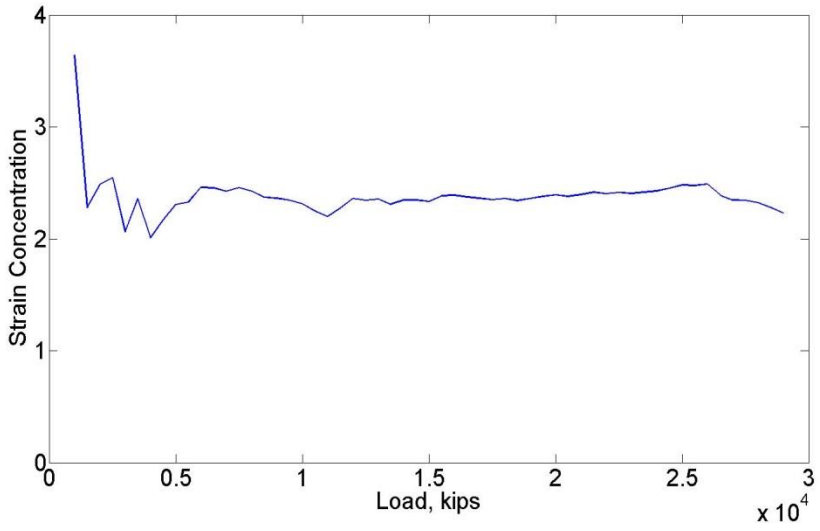

Figure 5.14. Strain concentration around circular hole

5.4 Summary

In this chapter, we studied damage growth in a quasi-isotropic CFRP panel which was used to represent a realistic aerospace component. A circular was cut into the center to mimic damage and PZT sensors were attached to measure the AE signals. Fiber optic sensors were also attached to measure the strain distribution.

The AE features measured, such as average frequency and duration, were analyzed but contained limited insight into the type of damage growth. Using a correlation technique, it was possible to see cluster formation during critical damage growth. Cluster sizes were seen to increase as the panel approached failure which shows a relationship between cluster size and the severity of damage. The final stage of failure was considered a "sudden-death" where the component rapidly failed and this failure is difficult to predict based on conventional AE analysis. Using the correlation technique, we were able to capture this by monitoring cluster growth which exponentially increase as we approach this region.

Strain measurement as the load increased can also show regions of damage growth. The development of damage changes the localized strain field and show up as strain concentrations.

Also, the presence of damage may cause the strain to decrease if that area is no longer able to carry any load. These subtle changes in the strain distribution can be used to monitor damage growth over a large area.

CHAPTER 6

Conclusions and Future Work

This dissertation focused on improving the detection of critical damage growth in CFRP panels. The problems investigated were analyzing damage growth in CFRP specimens due to static and fatigue loading, identifying critical damage growth in CFRP panels, and measuring changes in strain distribution during damage growth. Each research problem relied heavily on an experimental approach. Specimen tests, both static and fatigue, were done using ASTM standard specimens, presented in Chapter 4. The panel test utilized a large CFRP panel with center-drilled circular hole and fiber optic sensors were attached for strain measurement.

A summary for the individual research topics are listed below:

Static tests

- Extracted multiple hits that dominate AE windows at during rapid damage growth
- Average frequency of signals measure in cross-ply specimens increased at higher load around the fiber breakage region. For the quasi-isotropic specimens, the average frequency did not noticeably increase.
- Duration of signals measured in both cross-ply and quasi-isotropic specimens were similar but contained different frequency content.
- A correlation technique was developed and applied to the AE data and utilized localized damage growth to find cluster signals. The clusters only formed at high load around the critical damage growth region.

Fatigue tests

- The data from fatigue tests showed changes in some of the AE parameters, such as average frequency and duration but not enough to isolate the different failure mechanisms.
- The correlation technique was applied to the AE data and showed cluster formation early in the loading process and in the region close to failure.
- The cyclic loading caused the early damage, i.e. matrix cracking, to coalesce and propagate, giving rise to cluster formation
- More higher order clusters were seen due to the repetitive nature of fatigue loading.

Panel test

- Signals measured in a quasi-isotropic panel did not show much variation in the AE parameters.
- The AE signals measured in the panel were of the same nature as those measured during the specimen test.
- The frequency content of the AE signals varied between 100-400 kHz and duration was typically around 100μs.
- Clusters were seen to form within the damage growth region and increase up to failure.
- Fiber optic sensors were used to measure strain distribution.

The significance of each of the topics investigated is discussed in this chapter. Failure of composite materials is not well understand when it comes predicting when the specimen will fail. Although the different failure modes generate distinct AE signals, using the AE features to isolate the individual modes was not feasible. The original characteristics of the signals will

change due to interaction with damage. Having the ability to account for the effect of damage on AE signals is crucial if we are to use these features for source identification. Instead of solving extremely difficult inverse problems to solve this issue, a correlation technique to identify to onset of critical damage was developed. This technique made use of the effect of localized damage to help identify signals that are generated from the same location. Signals that occur at the location, having the same orientation, and the same path to a given sensor will have very similar features and will thus correlate. Applied to acoustic emissions from static tests, the correlation technique showed clusters forming within the region of critical damage growth. Cluster growth can be used as an indicator of critical damage growth for quasi-static testing. The same technique can be applied to fatigue loading but in addition to clusters that precede failure, there are some initial clusters due to localized matrix crack growth. Monitoring of distributed strain can be used to track the path of damage growth.

In addition to the research summarized above, some issues were encountered that could provide future areas of study. A few of these topics are listed below:

- Quantifying the effect of damage on the fundamental Lamb wave modes (symmetric and anti-symmetric)
- The effect of fatigue damage growth on strain distribution
- Further analysis on the AE features of clusters signals
- The effect fatigue loading on sensor performance

References

Aggelis, D. G., Barkoula, N. M., Matikas, T. E., & Paipetis, A. S. (2010). Acoustic emission monitoring of degradation of cross ply laminates. *Journal of the Acoustical Society of America, 127*(6), EL246-EL251. doi: 10.1121/1.3425752

Ahmadzadeh, G. R., Shirazi, A., & Varvani-Farahani, A. (2011). Damage Assessment of CFRP [90/±45/0] Composite Laminates over Fatigue Cycles. *Applied Composite Materials, 18*(6), 559-569. doi: 10.1007/s10443-011-9216-9

Appropedia. (2013). Composites in the Aircraft Industry. *http://www.appropedia.org/Composites_in_the_Aircraft_Industry*.

Arumugam, V., Sajith, S. (2011). Acoustic Emission Characterization of Failure Modes in GFRP Laminates Under Mode I Delamination. *Journal of Nondestructive Evaluation, 30*, 213-219.

Ativitavas, N. (2005). Identification of Fiber-reinforced Plastic Failure Mechanisms from Acoustic Emission Data using Neural Networks. *Journal of Composite Materials, 40*(3), 193-226. doi: 10.1177/0021998305053458

Berthelot, Jean-Marie. (2003). Transverse cracking and delamination in cross-ply glass-fiber and carbon-fiber reinforced plastic laminates: Static and fatigue loading. *Applied Mechanics Reviews, 56*(1), 111. doi: 10.1115/1.1519557

Bhat, C., Bhat, M. R., & Murthy, C. R. L. (2008). Characterization of Failure Modes in CFRP Composites -- An ANN Approach. *Journal of Composite Materials, 42*(3), 257-276. doi: 10.1177/0021998307086209

Bocchhieri, R. T., Schapery, R. A. (2004). Time-Dependent Deformation and Damage Growth in a Rubber-Toughened Fiber Composite. *Mechanics of Time-Dependent Materials, 8*, 137-167.

Bussiba, A., Kupiec, M., Ifergane, S., Piat, R., & Böhlke, T. (2008). Damage evolution and fracture events sequence in various composites by acoustic emission technique. *Composites Science and Technology, 68*(5), 1144-1155. doi: http://dx.doi.org/10.1016/j.compscitech.2007.08.032

D3039, ASTM. (2013). Standard Test Method for Tensile Properties of Polymer Matrix Composite Materials.

D3479, ASTM. (2013). Standard Test Method for Tension-Tension Fatigue of Polymer Matrix Composite Materials.

Daniel, I. M., Ishai, O. (1994). Engineering Mechanics of Composites Materials.

Evans, A. G., Fuller, E., R. (1974). Crack propagation in ceramic materials under cyclic loading conditions. *Metallurgical Transactions, 5*(1), 27-33.

Fidanboylu, K., Efendioglu, H.S. (2009). Fiber Optic Sensors and Their Applications. *5th International Advanced Technologies Symposium (IATS'09)*.

Gamstedt, E. K., & Sjogren, B. A. (2002). An experimental investigation of the sequence effect in block amplitude loading of cross-ply composite laminates. *International Journal of Fatigue, 24*(2-4), 437-446.

Giancane, S., Panella, F. W., & Dattoma, V. (2010). Characterization of fatigue damage in long fiber epoxy composite laminates. *International Journal of Fatigue, 32*(1), 46-53. doi: 10.1016/j.ijfatigue.2009.02.024

Hajikhani, M., Ahmadi, M. (2011). Strain energy release rate assessment in mode I delamination of foam core sandwich composites by acoustic emission. *Journal of Composite Materials, 45*(22), 2271-2277.

Hallett, S. R., Green, B. G., Jiang, W. G., & Wisnom, M. R. (2009). An experimental and numerical investigation into the damage mechanisms in notched composites. *Composites Part A: Applied Science and Manufacturing, 40*(5), 613-624. doi: 10.1016/j.compositesa.2009.02.021

Huang, Z. M. (2002). Fatigue life prediction of a woven fabric composite subjected to biaxial cyclic loads. *Composites Part a-Applied Science and Manufacturing, 33*(2), 253-266.

Johnson A. C., Hayes S., Jones F. (2012). The role of matrix cracks and fiber_matrix debonding on the stress transfer between fibre and matrix in a single fibre fragmentation test.pdf. *Composites Part A- Applied Science and Manufacturing, 43*(1), 65-72.

Jong, H. J. (2005). Transverse Cracking in a Cross-ply Composite Laminate - Detection in Acoustic Emission and Source Characterization. *Journal of Composite Materials, 40*(1), 37-69. doi: 10.1177/0021998305053507

Kleckers, T. (2007). Optical Strain Gauges vs. Electrical Strain Gauges: A Comparison.

Kumagai, S., & Shindo, Y. (2004). Experimental and Analytical Evaluation of the Notched Tensile Fracture of CFRP-Woven Laminates at Low Temperatures. *Journal of Composite Materials, 38*(13), 1151-1164. doi: 10.1177/0021998304042080

Lara-Curzio, E. (1998). On the matrix cracking stress and the redistribution of internal stresses in brittle-matrix composites. *Materials Science and Engineering: A, 250*(2), 270-278.

Li, Hui, Ou, Jinping, & Zhou, Zhi. (2009). Applications of optical fibre Bragg gratings sensing technology-based smart stay cables. *Optics and Lasers in Engineering, 47*(10), 1077-1084. doi: 10.1016/j.optlaseng.2009.04.016

Loutas, T. H., Panopoulou, A., Roulias, D., & Kostopoulos, V. (2012). Intelligent health monitoring of aerospace composite structures based on dynamic strain measurements. *Expert Systems with Applications, 39*(9), 8412-8422. doi: 10.1016/j.eswa.2012.01.179

Mieloszyk, M., Skarbek, L., Krawczuk, M., Ostachowicz, W., & Zak, A. (2011). Application of fibre Bragg grating sensors for structural health monitoring of an adaptive wing. *Smart Materials and Structures, 20*(12), 125014. doi: 10.1088/0964-1726/20/12/125014

Milne, I., Ritchie, R.O., & Karihaloo, B.L. (2003). *Comprehensive Structural Integrity*: Elsevier Science.

Momon, S., Moevus, M. (2010). Acoustic emission and lifetime prediction during static fatigue tests on ceramic-matrix-composite at high temperature under air. *Composites: Part A, 41*, 913-918.

Ogi, Keiji, Yashiro, Shigeki, Takahashi, Manabu, & Ogihara, Shinji. (2009). A probabilistic static fatigue model for transverse cracking in CFRP cross-ply laminates. *Composites Science and Technology, 69*(3-4), 469-476. doi: 10.1016/j.compscitech.2008.11.023

Raju, Azmi, A., & Prusty, B. (2012). Acoustic emission techniques for failure characterisation in composite top-hat stiffeners. *Journal of Reinforced Plastics and Composites, 31*(7), 495-516. doi: 10.1177/0731684412437986

Refahi Oskouei, Amir, Heidary, Hossein, Ahmadi, Mehdi, & Farajpur, Mehdi. (2012). Unsupervised acoustic emission data clustering for the analysis of damage mechanisms in

glass/polyester composites. *Materials & Design, 37*, 416-422. doi: 10.1016/j.matdes.2012.01.018

Reifsnider, K. L., & Jamison, R. (1982). Fracture of Fatigue-Loaded Composite Laminates. *International Journal of Fatigue, 4*(4), 187-197.

Reifsnider, K., & Majumdar, P. (2011). Material state change relationships to fracture path development for large-strain fatigue of composite materials. *Mechanics of Composite Materials, 47*(1), 1-10. doi: 10.1007/s11029-011-9183-0

Reifsnider, K.L., & Case, S.W. (2002). *Damage tolerance and durability of material systems*: Wiley Interscience.

Rose, J.L. (2004). Ultrasonic Waves in Solid Media.

Sanada, Hiroyuki, Sugita, Yutaka, & Kashiwai, Yoshio. (2012). Development of a multi-interval displacement sensor using Fiber Bragg Grating technology. *International Journal of Rock Mechanics and Mining Sciences, 54*, 27-36. doi: 10.1016/j.ijrmms.2012.05.020

Satapathy, M. R., Vinayak, B.G. (2013). Fatigue behavior of laminated composites with a circular hole under in-plane multiaxial loading. *Materials and Design, 51*, 347-356.

Sause, M. G. R., Gribov, A., Unwin, A. R., & Horn, S. (2012). Pattern recognition approach to identify natural clusters of acoustic emission signals. *Pattern Recognition Letters, 33*(1), 17-23. doi: 10.1016/j.patrec.2011.09.018

Scholey, J.J., Wilcox, P.D. (2006). Acoustic Emission in Wide Composite Specimens. *Advanced Materials Research, 13-14*, 325-332.

Shiuh-Chuan, H. (2009). Strain measurement of fiber optic sensor surface bonding on host material. *Transactions of Nonferrous Metals Society of China, 19*, 143-149.

Sousa, H. (2011). Design and implementation of a monitoring system applied to a long-span prestressed concrete bridge. *structural Concrete, 12*(2), 82-93.

Tuttle, M. E. (2004). *Structural Analysis of Polymeric Composite Materials*: Marcel Decker, Inc.

Wharmby, A. (2003). Observations on damage development in fibre reinforced polymer laminates under cyclic loading. *International Journal of Fatigue, 25*(5), 437-446. doi: 10.1016/s0142-1123(02)00118-4

Yang, J., Lee, H. (2012). An optical fiber guided ultrasonic excitation and sensing system for online monitoring of nuclear power plants. *AIP Conference Proceedings, 1640*(2012).

Appendix A

MATLAB code used for clustering

```
%finds AE signals within gage

clc
clear all

format long

a=load('graphite_data_table.txt');
test='real_test_1_2_';
f_ext='.txt';

amp_min=45;
amp_max=99;
t_sample=2.0e-7;
delta_t_valid = 0.00002;
HDT=0.000015;
HDT_pts=HDT/t_sample;
thresh=0.1;

event_peaks=19;
corr_sigs=10;
pts_beg=1000;
pts_end=2250;
perc=0.7;

k=1;
yy=1;
zz=1;

delta_value=15;  %(us) works for 11-18us

off_set=101; %offsets the waveform to zero out leading edge

[nrow,ncol]=size(a); %this section finds the gage waveforms

mm=1;
zz1=1;
zz2=1;
n=1;
p=1;
```

```
q=1;
for i=1:nrow-1;
   if a(i,2)==1
   if a(i,2)==1 && a(i+1,2)==2
      del_t=a(i+1,1)-a(i,1);
%       if abs(del_t)>=0.000015 && abs(del_t)<=0.000020 %delta t
      if abs(del_t)<=delta_t_valid
         if a(i,10)>=amp_min && a(i,10)<=amp_max
         wave_no1(n,1)=p;       %index for gage waveform for chan1
         wave_time(n,1)=a(i,1); %hit time
         wave_time(n,2)=a(i,2); %hit channel
         wave_time(n,3)=del_t;  %delta t of sensors
         wave_load1(n,1)=a(i,3); %load
         n=n+1;
         else end
      else end

   else end
   p=p+1;
   else end

   if a(i,2)==2
   if a(i,2)==2 && a(i+1,2)==1
      del_t=a(i+1,1)-a(i,1);
%       if abs(del_t)>=0.000015 && abs(del_t)<=0.000020
      if abs(del_t)<=delta_t_valid
         if a(i,10)>=amp_min && a(i,10)<=amp_max
         wave_no2(n,1)=q;       %index for gage waveform for chan2
         wave_time(n,1)=a(i,1); %hit time
         wave_time(n,2)=a(i,2); %hit channel
         wave_time(n,3)=-del_t;  %delta t of sensors
         wave_load2(n,1)=a(i,3); %load
         n=n+1;
         else end
      else end
   else end
   q=q+1;
   else end
end

wave_no11=wave_no1(wave_no1(:,1)~=0);      %this command collapses ch1 waveform # array
(only neccessary for linux)
```

```
wave_no22=wave_no2(wave_no2(:,1)~=0);      %this command collapses ch2 waveform # array
(only neccessary for linux)

wave_load11=wave_load1(wave_load1(:,1)~=0); %this command collapses ch1 waveform load
array (only neccessary for linux)
wave_load22=wave_load2(wave_load2(:,1)~=0); %this command collapses ch1 waveform load
array (only neccessary for linux)

gage_hits1=max(size(wave_no11)); %finds number of gage hits for ch1
gage_hits2=max(size(wave_no22)); %finds number of gage hits for ch2

for j=1:gage_hits1-corr_sigs; %cycles through ch1 gage waveforms

  load11(j,1)=wave_load11(1,1); %builds ch1 load array, always takes 1st element of original load
array
  table1(1,zz1)=wave_no11(1,1); %groups reference waveform with correlated waveforms, always
1st row of each column

    hit_no=num2str(wave_no11(1,1)); %the reference waveform is chosen, always the first
element in the wave_no11 array
    chan='1';
    file_name= strcat(test,chan,'_',hit_no,f_ext);
    y1=load(file_name);
    y11=y1(pts_beg:pts_end,1);

  for g=1:corr_sigs;          %this loop builds the element matrix that has n-columns, each
representing a waveform to be correlated
    hit_no1=num2str(wave_no11(g+1,1)); %chooses the waveforms that are after the reference,
reference waveform=wave_no(1,1)
    chan='1';
    file_name1= strcat(test,chan,'_',hit_no1,f_ext);
    waveform1=load(file_name1);
    element1(:,g)=waveform1(pts_beg:pts_end,1); %element matrix with n-columns, n = number of
signals to be correlated

  end

    for k=1:corr_sigs;        %loop to correlate reference to individual waveforms
    r_val1=xcorr(y11,element1(:,k),'coeff'); %correlates reference to each individual waveform in
the element matrix
    correl_coefficient1(1,k)=max(r_val1); %gathers the correlation coefficients, takes max
correlation value for each waveform
```

```
    if correl_coefficient1(1,k)<perc  %checks correlation value, if less than "perc", value is ignored
and made 0
      correl_coefficient1(1,k)=0;
    else
      table1(mm+1,zz1)=wave_no11(k+1,1); %if correlation value >perc, table is built to store
column of reference waveform followed by correlated waveform no.
      wave_no11(k+1,1)=0; %the waveform no is made 0 once it has been correlated
      wave_load11(k+1,1)=0; %the waveform load is made 0 once it has been correlated
      correl_coefficient1(1,k)=max(r_val1); %the real correlation value is chosen and stored
      mm=mm+1;
    end

  end

  match1=correl_coefficient1(correl_coefficient1(1,:)~=0); %correlation array is condensed to get
rid of zeros, see 115
  match11(j,1)=length(match1); %size on condensed match1 array is number of signals that
correlated at "perc" or better
  sum_of_sigs1(j)=match11(j,1)+1; %this checks to make sure the correct number of signals are
analyzed


  wave_no11(1,1)=0; %throws out reference waveform
  wave_load11(1,1)=0; %%throws out reference waveform load

  wave_no11=wave_no11(wave_no11(:,1)~=0); %condenses waveform no, gets rid of zeros, see
118
  wave_load11=wave_load11(wave_load11(:,1)~=0); %%condenses waveform no, gets rid of
zeros, see 119
  tot_wave1=length(wave_no11); %calculates number of remaining waveforms

  mm=1; %index for table1, see 93 & 117
  nn=length(table1(table1(:,zz1)~=0)); %finds length of each table column
  if nn<5                    %if number of correlated sigs <4, column is overwritten
    zz1=zz1;
  else zz1=zz1+1;
  end

    if tot_wave1<=corr_sigs      %if total number of sigs remaining is less that number to be
correlated, this section is ended
      break
    end
```

```
completion1=corr_sigs/tot_wave1        %calculates percentage of completion for this section
end

dis='stage1 complete'                  %displays completion message

save('/home/ULTRA/Travis/all_corr_data/graphite_dynamic_ch1.txt','match11','-ascii')
save('/home/ULTRA/Travis/all_corr_data/graphite_load_dynamic_ch1.txt','load11','-ascii')
mm=1;
for jj=1:gage_hits2-corr_sigs %this sections reads in the individual waveforms

    load22(jj,1)=wave_load22(1,1);
    table2(1,zz2)=wave_no22(1,1);

  for gg=1:corr_sigs;
    hit_no2=num2str(wave_no22(gg+1,1));
    chan='2';
    file_name2= strcat(test,chan,'_',hit_no2,f_ext);
    waveform2=load(file_name2);
    element2(:,gg)=waveform2(pts_beg:pts_end,1);
  end

    hit_no=num2str(wave_no22(1,1));
    chan='2';
    file_name= strcat(test,chan,'_',hit_no,f_ext);
    y2=load(file_name);
    y22=y2(pts_beg:pts_end,1);

    for kk=1:corr_sigs;
    r_val2=xcorr(y22,element2(:,kk),'coeff');
    correl_coefficient2(1,kk)=max(r_val2);

    if correl_coefficient2(1,kk)<perc
      correl_coefficient2(1,kk)=0;
    else
      table2(mm+1,zz2)=wave_no22(k+1,1);
      wave_no22(k+1,1)=0;
      wave_load22(k+1,1)=0;
      correl_coefficient2(1,k)=max(r_val1);
      mm=mm+1;
    end

  end
```

```
   match2=correl_coefficient2(correl_coefficient2(1,:)~=0);
   match22(jj,1)=length(match2);
   sum_of_sigs2(jj)=match22(jj,1)+1;

   wave_no22(1,1)=0;
   wave_load22(1,1)=0;

   wave_no22=wave_no22(wave_no22(:,1)~=0);
   wave_load22=wave_load22(wave_load22(:,1)~=0);
   tot_wave2=length(wave_no22);

   mm=1;
   nn=length(table2(table2(:,zz2)~=0));
   if nn<5
      zz2=zz2;
   else zz2=zz2+1;
   end

      if tot_wave2<=corr_sigs
         break
      end

completion2=corr_sigs/tot_wave2
end

dis2='stage2 complete'

save('/home/ULTRA/Travis/all_corr_data/graphite_dynamic_ch2.txt','match22','-ascii')
save('/home/ULTRA/Travis/all_corr_data/graphite_load_dynamic_ch2.txt','load22','-ascii')
```